U. S. Department of Energy grant DE-FG02-92ER25124
NUMERICAL CONFORMAL MAPPING: METHODS, APPLICATIONS, AND THEORY
Final Report - 10/20/95

Thomas K. DeLillo, Principal Investigator
Department of Mathematics and Statistics
Wichita State University
Wichita, KS 67260-0033
phone: 316-689-3974
email: delillo@twsuvm.uc.twsu.edu

Section 1 of this report, briefly summarizes research performed under this grant during the first two years 1992 to 1994 and makes some overall remarks. Section 2, summarizes research performed during the final year from September, 1994 through May 31, 1995, more fully. Section 3, summarizes travel, meetings, and other expenses supported by this grant during the final year. Enclosed are preprints of [CDH] and [DEH] which have been submitted for publication.

1. Brief summary of research, 1992 to 1994, and remarks.

Theoretical estimates for the ill-conditioning of the conformal mapping problems due to crowding were discussed in [DP1] and [De2] along with several computations. Further computations were reported in [De3]. Extensions of the ellipse method [DE3] via Faber series to overcome the ill-conditioning for regions with elongated sections were given in [DEP]. Use of analyticity conditions to develop methods for more general simply, doubly, and multiply connected regions was initiated [DP2], [Pf]. Applications of conformal mapping to the solution of the Dirichlet problem for the Laplace equation was studied in [De1] and comparison with iterative methods for integral equations is given in [DH].

A unifying theme in all this work is the use of conjugate-gradient-like methods to solve (nonsymmetric) linear systems resulting from the discretization of the identity plus a compact operator. This is also the case in the treatment of the biharmonic equation below. As a consequence, superlinear convergence rates are achieved and, for the conformal mapping applications, the matrix-vector multiplication may be done in $O(N \log N)$ with the FFT. Another important aspect of all this work has been the relation of the accuracy and conditioning of the problem to the geometry of the region.

Overall, we have found that these FFT-based conformal mapping methods can provide fast, accurate solutions to boundary value problems for the Laplace and the biharmonic equations for regions in the plane with smooth boundaries. The mathematical tools and theory are very interesting and touch on many topics of classical and current interest. However, these methods do suffer from the following drawbacks: unlike, for instance, methods based on direct integral equations [JS], [Poz], mixed boundary conditions which arise often in applications are difficult to treat; extensions to complicated or multiply-connected geometries are not as straight forward as, for instance, integral equation methods

[GGM], [GKM]; and regions with corners are difficult to treat accurately [De3], [DE2].

2. Summary of research, 1994 to 1995.

The main achievement of this last period of the grant has been the application of numerical conformal mapping to the solution of the biharmonic equation [CDH]. It is anticipated that this initial work will lead to many other results and applications. This will be discussed in *iv)*, below. Some additional progress has been made in the *i)* comparison of FFT methods, *ii)* analysis of methods for simply and doubly connected regions, and *iii)* applications to free boundary problems in ideal flow.

i) Comparison of FFT methods. In [We4] a new formulation of the ellipse method [DE3] is given. The method is an extension of Wegmann's original method for the disk [We1] and finds the boundary correspondence by a Newton-like method. The Newton updates are computed as solutions to Riemann-Hilbert problems using the conjugation operator on the ellipse. Like [We1], the method may fail to converge in many cases [De2], [DE1]. However, [We4] shows that convergence may be achieved by damping of higher order Fourier coefficients, with only a small loss in speed of convergence. We have applied this damping to our code for the original disk method [We1] and found that it now converges in many cases of practical interest, such as spline curves, where it previously failed. The method requires fewer FFTs per step than the equally reliable discrete interpolation method [Weg3] and is easier to code. We hope to eventually make Fortran and MATLAB code available for one or both of these methods.

ii) Analysis of methods for simply and doubly connected regions. This is joint work with John Pfaltzgraff of Chapel Hill. In [DP2], Fornberg's method [Fo1] is extended to the exterior and doubly-connected case [Fo2]. We have worked out more details of the operator equations, showing that each of these cases are of the form $I + R$ where R is a compact operator. Thus the conjugate gradient method converges superlinearly.

iii) Applications to free boundary problems. This is joint work with Alan Elcrat and Chenglie Hu of Wichita State U. Numerical algorithms were given in [DEH] for Helmholtz-Kirchhoff and reentrant jet flow, two classical free boundary problems for ideal flow past an obstacle. The methods are based on the Levi-Civita representation of the log-hodograph function and the use of FFTs for successive conjugation similar to the method of Timman for conformal mapping [DE2].

iv) The biharmonic equation. The initial phase of this work is reported in [CDH]. This is joint work with my graduate student, Mark Horn and with Raymond Chan of the Chinese University of Hong Kong. Boundary value problems for the biharmonic equation arise in plane elasticity problems and Stokes flow [GKM], [Musk], [Poz]. Unlike the Laplace equation, the biharmonic equation is not preserved under conformal transplantation. However, certain analytic functions can be transplanted to the computational region as we now decribe. The setup is described in [CDH] and follows the classical method in [Musk].

We wish to find the function u satisfying the biharmonic equation,

$$\Delta^2 u = 0$$

in a simply connected region Ω in the ζ–plane, $\zeta = \eta + i\mu \in \Omega$, with boundary values

$$u_\eta = G_1, \text{and } u_\mu = G_2$$

given on the boundary Γ of Ω. u can be represented as

$$u(\zeta) = Re(\bar{\zeta}\phi(\zeta) + \chi(\zeta)),$$

where $\phi(\zeta)$ and $\chi(\zeta)$ are analytic functions in Ω known as the *Goursat functions*. Letting $G = G_1 + iG_2$, the boundary conditions become

$$\phi(\zeta) + \zeta\overline{\phi'(\zeta)} + \overline{\psi(\zeta)} = G(\zeta), \quad \zeta \in \Gamma \tag{1}$$

where $\psi(\zeta) = \chi'(\zeta)$. The problem is to find ϕ and ψ analytic in Ω and satifying (1). Let $\zeta = f(z)$ be the conformal map from the unit disk to Ω, fixing $f(0)$. Then then with $d(z) := f(z)/\overline{f'(z)}$ and $\phi(z) := \phi(f(z))$, etc., equation (1) transplants to the disk as

$$\phi(z) + zd(z)\overline{\phi'(z)} + \overline{\psi(z)} = G(z), \quad |z| = 1. \tag{2}$$

Let

$$\phi(z) = \sum_{k=1}^{\infty} a_k z^k, \quad \psi(z) = \sum_{k=0}^{\infty} b_k z^k.$$

The problem is to find the a_k's and the b_k's. For $|z| = 1$, we have the Fourier series

$$d(z) := \frac{f(z)}{\overline{f'(z)}} = \sum_{k=-\infty}^{\infty} h_k z^k, \quad G(z) = \sum_{k=-\infty}^{\infty} A_k z^k.$$

Substituting into (2) gives a linear system of equations for the a_k's,

$$a_j + \sum_{k=1}^{\infty} k\bar{a}_k h_{j+k-1} = A_j, \; j = 1, 2, 3, \ldots \tag{3}$$

The b_k's can be easily computed from the a_k's. Note that the sum in (3) can be represented as the multiplication of the ka_k's by an infinite Hankel matrix. (A Hankel matrix is constant along the back-diagonals.)

Truncating gives our discretization of (3),

$$a_j + \sum_{k=1}^{n} k\bar{a}_k h_{j+k-1} = A_j, \; j = 1, \ldots, n \tag{4}$$

By taking real and imaginary parts, (4) may be written in the form

$$(I + HD)\underline{x} = \underline{r}, \tag{5}$$

where

$$\underline{x} = (Re\ a_1, \ldots, Re\ a_n, Im\ a_1, \ldots, Im\ a_n)^T,$$
$$\underline{r} = (Re\ A_1, \ldots, Re\ A_n, Im\ A_1, \ldots, Im\ A_n)^T,$$
$$D = \mathrm{diag}(1, 2, \ldots, n, 1, 2, \ldots, n),$$

and

$$H = \begin{pmatrix} H_r & H_i \\ H_i & -H_r \end{pmatrix}.$$

H_r and H_i are real $n \times n$ Hankel matrices with the entries constant on the kth back-diagonals and equal to $Re\ h_k$ and $Im\ h_k$, respectively. We have solved this system for several test cases using GCR and GMRES. (5) can be symmetrized to get

$$(I + M)\underline{y} = \underline{g}, \tag{6}$$

where $M = D^{1/2}HD^{1/2}$, $\underline{y} = D^{1/2}\underline{x}$, and $\underline{g} = D^{1/2}\underline{d}$. In [CDH] we show that M is compact and solve the normal equations for (6) by conjugate gradient. The matrix-vector multiplication can be done in $O(N \log N)$ using FFTs. The iterations converge rapidly. In our examples, we find numerically that $I + M$ is positive definite (when the discrete Fourier coefficients h_k are set to 0 for $k > n$), however we have not been able to prove this in general. We can prove the following theorem on the superlinear convergence:

Theorem. *Let Γ be analytic and $A = I + M$ be positive definite. Then there exists an $R < 1$ such that the error vector e_q at the qth step of conjugate gradient satisfies*

$$\|e_q\|_A \leq C^q \kappa^k R^{q^2} \|e_0\|_A$$

where κ is the condition number of the matrix $I + M$ and C and k are constants depending only on f.

Somewhat slower superlinear convergence can also be shown for boundaries with less smoothness. We are planning to present these results in a future paper. We also hope to prove theorems of the following sort for the accuracy of ϕ_n, the approximation to ϕ:

Theorem. *Let Γ be analytic and let the boundary data G be analytic. Then there is an $R < 1$ such that*

$$\|\phi - \phi_n\|_\infty = O(R^n).$$

We have extended the above setup to the case where f is the conformal map from an ellipse $E : \rho z + 1/(\rho z), |z| = 1$ to Ω [DE3], [Weg4]. Now ϕ and ψ have Laurent series

$$\phi(f(z)) = \sum_{k=-\infty}^{\infty} a_k z^k, \quad \psi(f(z)) = \sum_{k=-\infty}^{\infty} b_k z^k, \quad |z| = 1.$$

Applying the analyticity conditions from [DE3], [DEP] to ϕ and ψ gives

$$a_k = \rho^{2k} a_{-k},\ b_k = \rho^{2k} b_{-k}.$$

Substituting into the boundary conditions (2) and eliminating the b_k's gives the following equation for the a_k's, $k \geq 1$,

$$a_j(1-\rho^{-4j}) + \rho^{-1} \sum_{k=1}^{\infty} k\overline{a}_k((h_{j+k-1} + \rho^{-2(j+k)} h_{-(j+k)-1}) - (\rho^{-2j} h_{k-j-1} + \rho^{-2k} h_{j-k-1}))$$

$$= A_j - \rho^{-2j} A_{-j}, j \geq 1.$$

Truncating this system leads to a discrete system roughly of the form block Hankel plus Toeplitz. Preconditioned conjugate gradient methods along the lines of [CS], [Ch] should lead to fast methods.

Further generalizations are possible to cases where f is a Faber series map from a cross-shaped or spoke-like region [DEP], an annulus, or, perhaps, a multiply-connected region. In [GGMa] the Sherman-Lauricella equation is solved for spoke-like regions which provide difficult regions for plane stress and plane strain problems. It is hoped that our Faber series methods may have some advantages for such extreme regions, however, the numerics gets increasingly complicated. The classic text [Musk] has a wealth of examples and material from 2-dimensional elasticity which are ripe for the application of modern techniques of numerical and computational complex analysis. For instance, Riemann-Hilbert problems for regions with cracks are also discussed. It should be possible to combine FFTs, conformal mapping, and Schwarz alternating procedures to compute, for instance, stress intensity factors efficiently.

3. Summary of travel and other expenses, 1994 to 1995

This covers the period from September, 1994 through the conclusion of the grant on May 31, 1995: A poster session was presented on this work at the DOE Applied Math meeting in Albuquerque, 2/27 to 3/1/95. I visited M. Eiermann and E. Wegert at the University of Freiberg, Freiberg, Germany from 3/19 to 3/22/95 and gave a talk on *Numerical conformal mapping methods for multiply-connected regions and some applications.* I visited R. Wegmann at the Max Planck Institute fur Astrophysik in Munich from 3/22 to 3/25/95. From 3/26 to 4/1/95, I attended the conference organized by D. Gaier and R. Varga on Konstruktive Verfahren in der komplexen Analysis at the Mathematisches Forschungsinstitut Oberwolfach, Germany and gave an invited talk on joint work with R. Chan and M. Horn on *The numerical solution of the biharmonic equation by conformal mapping.* I also attended the Midwest Numerical Analysis Day organized by K. Atkinson and his colleagues at the University of Iowa on 4/29/95 where my PhD student M. Horn talked on our joint work on the biharmonic equation. The above trips were partially funded by this grant.

The following related visits were not funded by this grant: I gave an invited expository talk on *An introduction to numerical conformal mapping,* at the Mathematics Colloquium,

University of North Florida, 4/21/95. I also visited John Pfaltzgraff at Chapel Hill from 6/17/95 to 6/27/95 and Raymond Chan visited me in Wichita from 8/10/95 to 8/25/95. During these visits further work was done related to this grant.

Since summer 1995 support was also available from NSF EPSCoR grant OSR-9255223 about $ 3064 of was rebudgeted to purchase software for use by colleagues and graduate students. 5 copies of MATLAB for PCs and a MATLAB license for the department SUN Sparc 5 workstation were purchased. Also 4 Fortran and 2 C++ compilers were purchased for PCs. MATLAB codes have been used on PCs and the workstation for [CDH]. It is hoped that MATLAB and Fortran versions of our conformal mapping codes may eventually be made available.

References

[CDH] R. H. Chan, T. K. DeLillo, and M. A. Horn, *The numerical solution of the biharmonic equation by conformal mapping,* submitted for publication.

[CS] R. H. Chan and G. Strang, *Toeplitz equations by conjugate gradients with circulant preconditioner,* SIAM J. Sci. Stat. Comput., 10 (1989) 104–119.

[Ch] R. H. Chan, *Circulant preconditioners for Hermitian Toeplitz systems,* SIAM J. Matrix Anal. Appl., 10 (1989) 542–550.

[De1] T. K. DeLillo, *On the use of numerical conformal mapping methods in solving boundary value problems for the Laplace equation,* in: R. Vichnevetsky, D. Knight, and G. Richter, eds., Advances in Computer Methods for Partial Differential Equations- VII, Seventh IMACS Symposium Proceedings, Rutgers University, (1992) 190–194.

[De2] T. K. DeLillo, *The accuracy of numerical conformal mapping methods: a survey of examples and results,* SIAM J. Numer. Anal., 31 (1994) 788–812.

[De3] T. K. DeLillo, *Comparisons of some numerical conformal mapping methods,* in: W. F. Ames, ed. Proceedings of the 14th IMACS World Congress on Computation and Applied Mathematics, Vol. 1, Georgia Institute of Technology (1994) 115–118.

[De4] T. K. DeLillo, *Comparison of some numerical conformal mapping methods,* in preparation.

[DE1] T. K. DeLillo and A. R. Elcrat, *A comparison of some numerical conformal mapping methods for exterior regions,* SIAM J. Sci. Statis. Comput., 12 (1991) 399–422.

[DE2] T. K. DeLillo and A. R. Elcrat, *Numerical conformal mapping methods for exterior regions with corners,* J. Comput. Phys., 108 (1993) 199–208.

[DE3] T. K. DeLillo and A. R. Elcrat, *A Fornberg-like conformal mapping method for slender regions,* J. Comput. Appl. Math., 46 (1993) 49–64.

[DEH] T. K. DeLillo, A. R. Elcrat, and C. Hu, *Helmholtz-Kirchhoff and reentrant jet flows using Fourier series,* submitted for publication.

[DEP] T. K. DeLillo, A. R. Elcrat, and J. A. Pfaltzgraff, *Numerical conformal mapping methods based on Faber series,* submitted for publication.

[DH] T. K. DeLillo and M. A. Horn, *The numerical solution of the Laplace equation in slender, simply-connected domains by integral equation and conformal mapping methods,* in preparation.

[DP1] T. K. DeLillo and J. A. Pfaltzgraff, *Extremal distance, harmonic measure and numerical conformal mapping,* J. Comput. Appl. Math., 46 (1993) 103–113.

[DP2] T. K. DeLillo and J. A. Pfaltzgraff, *Numerical conformal mapping methods for exterior, doubly, and multiply-connected regions,* in preparation.

[Fo1] B. Fornberg, *A numerical method for conformal mappings,* SIAM J. Sci. Statis. Comput., 1 (1980) 386–400.

[Fo2] B. Fornberg, *A numerical method for conformal mapping of doubly connected regions,* SIAM J. Sci. Statis. Comput., 4 (1984) 771–783.

[GGMa] A. Greenbaum, L. Greengard, and A. Mayo, *On the numerical solution of the biharmonic equation in the plane,* Physica D, 60 (1992) 216–225.

[GGM] A. Greenbaum, L. Greengard, and G. B. McFadden, *Laplace's equation and the Dirichlet-Neumann map in multiply connected domains,* J. Comput. Phys., 105 (1993) 267–278.

[GKM] L. Greengard, M. C. Kropinski, and A. Mayo, *Integral equation methods for Stokes flow and isotropic elasticity in the plane,* Courant Mathematics and Computing Laboratory Report 95-006 (1995).

[Musk] N. I. Muskhelishvili, Some Basic Problems of the Mathematical Theory of Elasticity, P. Noordhoff Ltd, Groningen, Holland (1953).

[JS] M. A. Jaswon and G. T. Symm, Integral Equation Methods in Potential Theory and Elastostatics, Academic Press, New York (1977).

[Pf] J. A. Pfaltzgraff, *Analyticity conditions for numerical conformal mapping,* in: W. F. Ames, ed., Proceedings of the 14th IMACS World Congress on Computation and Applied Mathematics, Vol. 1, Georgia Institute of Technology, (1994) 397–399.

[Poz] C. Pozrikidis, Boundary Integral and Singularity Methods for Linearized Viscous Flow, Cambridge U. Press (1992).

[Weg1] R. Wegmann, *Convergence proofs and error estimates for an iterative method for conformal mapping,* Numer. Math., 44 (1984) 435–461.

[Weg2] R. Wegmann, *On Fornberg's numerical method for conformal mapping,* SIAM J. Numer. Anal., 23 (1986) 1199–1213.

[Weg3] R. Wegmann, *Discrete Riemann-Hilbert problems, interpolation of simply closed curves, and numerical conformal mapping,* J. Comput. Appl. Math., 23 (1988) 323–352.

[Weg4] R. Wegmann, *Fast conformal mapping of an ellipse to a simply connected region,* preprint.

Submitted for publication

Helmholtz-Kirchhoff and Reentrant Jet Flows Using Fourier Series

Thomas K. DeLillo, Alan R. Elcrat, and Chenglie Hu
Department of Mathematics & Statistics
Wichita State University
Wichita, Kansas 67260-0033, U.S.A.

§1. INTRODUCTION

In this paper we revisit a classical topic in ideal flow hydrodynamics. In particular we are concerned with two dimensional, incompressible, nonviscous, irrotational steady flows past obstacles in which a wake or cavity is formed in which the fluid is assumed to be at rest at constant pressure. We will present numerical algorithms for the problems under discussion and give a sample of computational results.

Consider that a fixed curved obstacle AB (see Figure 1) and a flow in which a wake or a cavity forms behind AB. We assume the following conditions:

A) The flow is bounded by AB and free streamlines Σ and Σ^* detaching from A and B respectively; (Note that, in general, only with boundary layer analysis can we determine the detaching points.)

B) The flow speed U on Σ and Σ^* is constant.

$C)_1$ Σ and Σ^* extend downstream to the infinity and enclose within it a wake of constant pressure (Figure 1(a)). (Note, however, that intersection of the free streamlines is not excluded by the model.) Or,

$C)_2$ Σ and Σ^* turn back, the flow forming a reentrant jet (Figure 1(b)).

In order to preserve a steady flow, it is assumed, when assumption $C)_2$ is used, that the jet is not interrupted by striking the rear of the obstacle, but rather lies on a second sheet of the flow surface. The flow region is thus simply-connected on a two-sheeted Riemann surface over the z-plane with infinity of the flow plane (denoted by I) being an interior point and the point at infinity on the jet (denoted by E) being a boundary point (Figure 1(b)).

$A)$, $B)$, and $C)_1$ define the Helmholtz-Kirchhoff flow, herein denoted the H-K flow, while $A)$, $B)$, $C)_2$ give the reentrant model, denoted the R-J flow. The "cavitation number",

$$\sigma = \frac{P_\infty - P_c}{\frac{1}{2}\rho U^2} \left(= \frac{V^2 - U^2}{U^2} \text{ using the Bernoulli equation} \right)$$

where P_∞, P_c are the pressure at infinity and the vapor pressure, respectively, and ρ is the density of the fluid (V and U are the cavity velocity and the velocity at infinity respectively). For the H-K model $\sigma = 0$, whereas in real flows σ is usually positive and it is this fact which motivated the invention of various "underpressure models" such as the R-J model over the years. Any such model must, by necessity, introduce some

artificial features into the flow, and cannot be expected to be correct in all details, but the reentrant jet model is particularly elegant and appealing, and we believe this justifies our return to this classical idea.

Older work on free streamline models in general and the R-J model in particular, is surveyed in [1], [2], [3], and [13]. More recently the H-K flow for curved obstacles has been studied by [6] using ideas in [17], and polygonal obstacles have been studied in [7], [8], and [9]. The numerical approach for the H-K model presented here is closely related to various "Fourier Series" methods for finding conformal maps [18], and, in fact, the functional equation which is iterated is almost identical to that used in Timman's method (see [19] and [15]). The method we give is efficient, can be made as accurate as desired by increasing the number of mesh points, and can be applied to rather general geometries. Corners can be included using ideas analogous to those in [16] but we have not included this here. There has been little numerical work for the reentrant jet model, and none, as far as we know, for general curved geometries. The procedures that we use may be thought of as complementary to the theoretical work which has been done in [4] and [5]. It should be remarked, however, that existing theoretical work is largely restricted to symmetric problems, and existence and uniqueness questions for the nonsymmetric problems discussed here are still open.

The cavitation number is a free parameter in the R-J model and in a complete physical description of a flow problem it must be determined as a part of the problem. We are not concerned with this problem here, but the methods we introduce may be useful in future work. We mention, for example, [11], [12], and [14].

The paper is organized as follows. Section 2 is devoted to the analytical formulation of the models. During the process of our work, we found some inconsistencies in some formulae given in [2] for the R-J model, and consequently, we have given derivations here. Our numerical formulation and computed examples are given respectively in Sections 3 and 5. The convergence of our numerical procedures will be discussed in section 4.

§2 THE ANALYTICAL REPRESENTATION OF THE MODELS

Let the region in the z-plane occupied by the fluid be denoted by R. The positive x-axis is taken in the direction of the incident uniform flow. Let $w(z)=\varphi(x,y)+i\psi(x,y)$ $i=\sqrt{-1}$, be the complex potential (thus $\varphi(x,y)$ is the velocity potential and $\psi(x,y)$ is

the stream function of the flow). $w(z)$ is defined up to an additive constant and is analytic in the interior of R. We may take $w(0)=0$. The complex velocity is thus $\frac{dw}{dz} = qe^{-i\theta}$, where q and θ are respectively the magnitude and the inclination of the velocity vector at a point $z \in R$.

(*a*) **The Formulation of H-K Model.** The central idea of the Levi-Civita representation is to introduce the so called logarithmic hodograph variables defined by (assuming the free streamline velocity to be unity)

$$Q(z) = iLog(\frac{dw}{dz}) = \theta(z) + iLog\ q(z), \tag{2.1}$$

which is analytic in R. Denote by Γ the semi-circular region in the ζ-plane ($\zeta = \xi + i\eta$), Γ: $|\xi| < 1$, $\eta > 0$. The complex potential $w(z)$ takes the flow region into the full z-plane slit along the positive x-axis. One then sees that the potential plane is mapped conformally onto Γ by

$$w(\zeta) = M[\cos(S_0) - \tfrac{1}{2}(\zeta + 1/\zeta)]^2 \tag{2.2}$$

such that $\zeta_A = 1$, $\zeta_B = -1$, $\zeta_E = 0$, and $\zeta_0 := e^{iS_0}$ correspond the origin of the w-plane (Figure 2), where constants M and S_0 need to be determined.

Now let $z(\zeta)$ be the conformal map (whose exact expression is never needed for H-K model) from Γ to R and define $\omega(\zeta) = Q(z(\zeta))$ (known as Levi-Civita parameterization of the *log*-hodograph function defined by (2.1)); this function is real on the real axis since $\frac{dw}{dz} = 1$ on the free boundaries. Therefore the reflection principle allows $\omega(\zeta)$ to be extended analytically to the lower-half unit circle. Applying the Schwarz-Poisson formula then gives, noting $\theta(e^{is}) = \theta(e^{-is})$,

$$\omega(\zeta) = \frac{1}{2\pi}\int_0^{2\pi} \theta(e^{is})\,\frac{e^{is}+\zeta}{e^{is}-\zeta}\,ds = \frac{1}{\pi}\int_0^{\pi} \theta(e^{is})\,\frac{1-\zeta^2}{1-2\zeta\cos(s)+\zeta^2}\,ds. \tag{2.3}$$

To determine $\omega(\zeta)$ completely, let l, $0 < l < L$, be arc length measured along the obstacle AOB from A to B and the inclination of the tangent on the boundary AOB be denoted by $\Psi(l)$. For a given flow, let $l(s)$ be boundary correspondence between AOB and the semi-circle, $\zeta = e^{is}$ $0 \le s \le \pi$, in ζ-plane. Then from

$$\theta(e^{is}) = \begin{cases} \Psi[l(s)] - \pi & 0 \le s < S_0 \\ \\ \Psi[l(s)]. & S_0 < s \le \pi \end{cases} \tag{2.4}$$

and (2.3), one gets

$$\omega(\zeta) = \Omega(\zeta) - \int_0^{S_0} \frac{1-\zeta^2}{1-2\zeta\cos(s)+\zeta^2}\, ds, \tag{2.5}$$

with the definition $(\Theta(e^{is}) := \Psi[l(s)])$

$$\Omega(\zeta) = \Theta(\zeta) + iT(\zeta) = \frac{1}{\pi}\int_0^{\pi} \Psi[l(s)]\, \frac{1-\zeta^2}{1-2\zeta\cos(s)+\zeta^2}\, ds. \tag{2.6}$$

Noting that with $t = e^{is}$

$$\int_\alpha^\beta \frac{1-\zeta^2}{1-2\zeta\cos(s)+\zeta^2}\, ds = \frac{i}{\zeta}\int_{e^{i\alpha}}^{e^{i\beta}} \frac{1-\zeta^2}{(t-\zeta)(t-\frac{1}{\zeta})}\, dt = i\Big(Log\frac{\zeta(e^{i\beta}-\zeta)}{\zeta-1} - Log\frac{\zeta(e^{i\alpha}-\zeta)}{\zeta-1}\Big), \tag{2.7}$$

we obtain

$$\omega(\zeta) = \Omega(\zeta) + iLog\, \frac{\zeta - e^{iS_0}}{\zeta e^{iS_0}-1}\,. \tag{2.8}$$

For a given function $\Psi(l)$, Ω, and hence ω, are completely determined once $l(s)$ is known. First $\omega(0) = 0$, together with (2.6) and (2.8), implies

$$S_0 = \Theta(0) = \frac{1}{\pi}\int_0^{\pi} \Psi[l(s)]\, ds. \tag{2.9}$$

Noting (2.1), one gets

$$\frac{dz}{ds} = ie^{is}e^{i\omega(e^{is})}w'(e^{is}), \tag{2.10}$$

from which, (2.2), and (2.8)

$$\frac{dl}{ds} = \Big|\frac{dz}{ds}\Big| = 4Me^{-T(e^{is})}\sin^2\Big(\frac{s+S_0}{2}\Big)\, \sin s, \tag{2.11}$$

or upon integration,

$$l(s) = 4M\int_0^{s} e^{-T(e^{i\theta})}\sin^2\Big(\frac{\theta+S_0}{2}\Big)\, \sin\theta d\theta \tag{2.12}$$

with

$$M = \frac{L}{4}\Big\{\int_0^{\pi} e^{-T(e^{is})}\sin^2\Big(\frac{s+S_0}{2}\Big)\, \sin s ds\Big\}^{-1}. \tag{2.13}$$

In view of (2.6) and (2.9), (2.12) can be thought of as an operator for $l(s)$,

$$l(s) = F[l(s);\, \Psi(l(s)), S_0], \tag{2.14}$$

where F is biven by (2.12). The analytic formulation for the H-K model is now completed.

(*b*) The Formulation of R-J Model. We will keep the same notation used for H-K model. The exact meaning can be seen easily from the context. First, the complex potential $w(z)$ can be made single-valued if the z-plane is cut along the streamline EDI (see Figure 3). The w-image of the cut flow region is thus a Riemann surface bounded by the slit positive real axis, *i.e.*, $OBEAO$ (Figure 3(*a*)). The slits IDE in the upper and lower parts of the w-plane are respectively images of the upper and lower parts of the cut IDE in the z-plane. Considered as a Riemann surface, the complete w-image consists of infinitely many such congruent sheets joined pairwise at the winding point w_D along DI and DE. Note here also that the "point" D on the upper and lower slits need not lie on a vertical line since, in general, the circulation around the cavity is not zero. The w-image region is then mapped into the ζ-plane so that the origin and e^{iS_0} on the ζ-plane correspond to the vertices E and O on the w-plane (Figure 3(*b*)).

The Osgood-Caratheodory extension of the Riemann mapping theorem ensures that there is a unique analytic function $z(\zeta)$ mapping Γ conformally onto the flow region such that $z(0)=E, z(-1)=B,$ and $z(1)=A$. In the vicinity of ζ_I, one has an expansion

$$z(\zeta)=\frac{r}{\zeta-\zeta_I}+P(\zeta-\zeta_I), \quad r\neq 0, \tag{2.15}$$

where $P(\zeta-\zeta_I)$ is regular at ζ_I and $P(0)\neq 0$. (P appearing in some of the following expressions will be tacitly assumed to satisfy similar assumptions.) $w(\zeta):=w(z(\zeta))$ is then the desired mapping from Γ to the w-image region. Using the Schwarz-Christoffel transformation extended to Riemann surfaces [10], it can be shown that

$$\frac{dw}{d\zeta}=M\,\frac{(\zeta^2-1)(\zeta-e^{iS_0})(\zeta-e^{-iS_0})(\zeta-\zeta_D)(\zeta-\bar{\zeta}_D)(\zeta-1/\zeta_D)(\zeta-1/\bar{\zeta}_D)}{\zeta(\zeta-\zeta_I)^2(\zeta-\bar{\zeta}_I)^2(\zeta-1/\zeta_I)^2(\zeta-1/\bar{\zeta}_I)^2}, \tag{2.16}$$

where M is a real constant. We define

$$Q_1(z)=iLog(\,\frac{1}{V}\frac{dw}{dz}\,)=\theta(z)+iLog(\,\frac{q(z)}{V}\,), \tag{2.17}$$

where V denotes the (constant) speed on the free streamlines. $Q_1(z)$ is analytic in the interior of the flow region except at stagnation point D. It is easily seen that $\omega(\zeta):=Q_1(z(\zeta))$ is multi-valued and has a following expression at ζ_D

$$\omega(\zeta)=iLog(\zeta-\zeta_D)+P(\zeta-\zeta_D). \tag{2.18}$$

Then

$$\omega(\zeta) = iLog\,\frac{(\zeta-\zeta_D)(\zeta\overline{\zeta}_D-1)(\zeta-e^{iS_0})}{(\zeta-\overline{\zeta}_D)(\zeta\zeta_D-1)(\zeta e^{iS_0}-1)}+\Omega(\zeta). \tag{2.19}$$

In fact,

$$f(\zeta) = \omega(\zeta) - iLog(\zeta-\zeta_D) - iLog\frac{(\zeta\overline{\zeta}_D-1)}{(\zeta-\overline{\zeta}_D)(\zeta\zeta_D-1)} \tag{2.20}$$

is single-valued and analytic in Γ (note that the third term of (2.20) has no singularities in Γ). The reason for introduction of the third term in (2.20) is twofold. First, $f(e^{is})$ has the same real part as $\omega(e^{is})$ for $0 \le s \le \pi$, and f is real in (-1,1). $f(\zeta)$ may, therefore, be analytically extended to the lower half of the circle and expressed by

$$f(\zeta) = \frac{1}{\pi}\int_0^{\pi}\theta(e^{is})\,\frac{1-\zeta^2}{1-2\zeta\cos(s)+\zeta^2}\,ds. \tag{2.21}$$

If the branch of $\omega(\zeta)$ is chosen so that

$$Re[\omega(e^{is})] = \theta(e^{is}) = \begin{cases} \Psi[l(s)]-\pi & 0 \le s < S_0 \\ \\ \Psi[l(s)] & S_0 < s \le \pi, \end{cases} \tag{2.22}$$

then

$$f(\zeta) = \Omega(\zeta) + iLog\,\frac{\zeta-e^{iS_0}}{\zeta e^{iS_0}-1},$$

which, together with (2.20), gives (2.19).

The central equations for the R-J model can now be stated as follows:

$$1)\quad \omega(\zeta_I) = iLog\left(\frac{U}{V}\right); \tag{2.23}$$

$$2)\quad \operatorname*{Res}_{\zeta=\zeta_I}\frac{dz}{d\zeta} = 0; \tag{2.24}$$

$$3)\quad Im\left\{\lim_{\zeta\to\zeta_I}\frac{d}{d\zeta}\left[(\zeta-\zeta_I)^2\frac{dw}{d\zeta}\right]\right\} = H/2\pi, \tag{2.25}$$

where H is the prescribed circulation;

$$4)\quad \frac{dl}{ds} = \frac{M_1}{V}e^{-T(e^{is})}\nu(s;S_0,\zeta_I,\zeta_D) \tag{2.26}$$

with

$$\nu(s;\,S_0,\zeta_I,\zeta_D) := \left|\frac{(e^{2is}-1)(e^{i(s+s_0)}-1)^2(e^{is}-\overline{\zeta}_D)^2(e^{is}\zeta_D-1)^2}{(e^{is}-\zeta_I)^2(e^{is}-\overline{\zeta}_I)^2(e^{is}\zeta_I-1)^2(e^{is}\overline{\zeta}_I-1)^2}\right|$$

$$= 8 \sin s \sin^2 \frac{s+S_0}{2} \frac{[1+d^2-2d\cos(s+\beta)]^2}{[1+h^2-2h\cos(s-\alpha)]^2[1+h^2-2h\cos(s+\alpha)]^2}$$

assuming $\zeta_I = he^{i\alpha}$, $\zeta_D = de^{i\beta}$; and

$$5) \quad M_1 = VL\{\int_0^{\pi} e^{-T(e^{is})} \nu(s; S_0, \zeta_I, \zeta_D) ds\}^{-1}. \tag{2.27}$$

Equations (2.23) – (2.25) and (2.27) determine parameters ζ_D, ζ_I, S_0, M_1 and hence the entire flow once the boundary correspondence $l(s)$ is known. Integrating equation (2.26) defines another functional equation

$$l(s) = G[l(s); \Psi(l(s)), S_0, \zeta_I, \zeta_D]. \tag{2.28}$$

Equations (2.23)-(2.26) can be established as follows. First (2.23) simply states that the flow velocity at infinity is U. To account for (2.24), we recall that $z'(\zeta)$ (see (2.15)) has a pole of exact order two at ζ_I, where $z'(\zeta)$ thus has a residue zero. To prove (2.25), first we need an expansion of $w(z)$ in the neighborhood of I, the point at infinity. Considering any circuit around the cavity, the value of $w(z)$ after such a circuit differs from its starting value by a complex constant k, which is independent of the path and the starting point. In particular, the change in value ($Im(k)$) of ψ must be non-zero to account for the jets, while the change in value ($Re(k)$) of φ is equal to the circulation about the cavity. $w(z) - (k/2\pi i) Logz$ is, therefore, single valued near I, and hence, since $\lim_{z \to I} w'(z) = U$,

$$w(z) = Uz + \frac{k}{2\pi i} Logz + P(\tfrac{1}{z}), \tag{2.29}$$

where the coefficient of $Logz$ has been adjusted so that $H = \oint grad\varphi dz = Re(k)$. One then has (noting (2.15))

$$w'(\zeta) = w'(z(\zeta))z'(\zeta) = -\frac{Ur}{(\zeta-\zeta_I)^2} - \frac{k}{2\pi i(\zeta-\zeta_I)} + P(\zeta-\zeta_I). \tag{2.30}$$

Then

$$Im\{\operatorname*{Res}_{\zeta = \zeta_I} \frac{dw}{d\zeta}\} = LHS \text{ of } (2.25) = Im(-\frac{k}{2\pi i}) = \frac{H}{2\pi}.$$

Finally to prove (2.26), we start with (2.16), which can be rewritten as

$$\frac{dw}{d\zeta} = M \frac{|\zeta_I|^4}{|\zeta_D|^2} \frac{(\zeta^2-1)(\zeta-e^{iS_0})(\zeta-e^{-iS_0})(\zeta-\zeta_D)(\zeta-\overline{\zeta}_D)(\zeta\zeta_D-1)(\zeta\overline{\zeta}_D-1)}{\zeta(\zeta-\zeta_I)^2(\zeta-\overline{\zeta}_I)^2(\zeta\zeta_I-1)^2(\zeta\overline{\zeta}_I-1)^2}. \tag{2.31}$$

As before

$$\frac{dl}{ds}=\left|\frac{dz}{ds}\right|=\frac{1}{V}\left|e^{i\omega(e^{is})}w'(e^{is})\right|; \tag{2.32}$$

(2.19) implies

$$\left|e^{i\omega(e^{is})}\right|=e^{-T(e^{is})}\left|\frac{(e^{is}-\zeta_D)(e^{is}\overline{\zeta}_D-1)(e^{i(s+S_0)}-1)}{(e^{is}-\overline{\zeta}_D)(e^{is}\zeta_D-1)(e^{is}-e^{iS_0})}\right|,$$

which, combining (2.31) and (2.32), gives (2.26) with

$$M_1=|M|\frac{|\zeta_I|^4}{|\zeta_D|^2}. \tag{2.33}$$

((2.33) clarifies the formulation given in [2], where the definition of M is not consistent comparing (23.8) on $P371$ with (33.11) on $P397$). The analytic formulation of H-J model is completed.

Once $\omega(\zeta)$ is determined, the forces exerted on the obstacle can be calculated by

$$X+iY=-\frac{i\rho V}{2}\oint e^{i\omega(\zeta)}\frac{dw}{d\zeta}\,d\zeta\,, \tag{2.34}$$

with X and Y representing drag and lift forces respectively. The integral is taken counterclockwise about any simple circuit containing $|\zeta|=1$. For H-K flow ($U=V=1$), using residue theorem and the expansion

$$e^{i\omega(\zeta)}=1+i\zeta\omega'(0)+\frac{\zeta^2}{2}\left[i\omega''(0)-\omega'(0)^2\right]+\cdots,$$

one gets

$$X+iY=\frac{\pi}{4}M\{\omega'(0)^2+i[4\omega'(0)\cos S_0-\omega''(0)]\} \tag{2.35}$$

with

$$\omega'(0)=\Omega'(0)-2\sin S_0\,,\quad \omega''(0)=\Omega''(0)-2\sin 2S_0\,,$$

while for the R-J flow, one has

$$X=\rho VJ(U-V\cos\gamma),\quad Y=-\rho V(UJ\sin\gamma+H), \tag{2.36}$$

where $\gamma:=\omega(0)$ is called the limiting direction, and J is called the jet width, and is defined by

$$J:=-\frac{e^{-i\gamma}}{2iV}\oint e^{i\omega(\zeta)}\frac{dw}{d\zeta}\,d\zeta=-\frac{\pi M}{V}, \tag{2.37}$$

where the circuit is about the origin.

The free streamline is determined by

$$z(\xi) = \mu \int_{e^{iS_0}}^{\xi} e^{i\omega(\zeta)} \frac{dw}{d\zeta}\, d\zeta \qquad -1 \le \xi \le 1, \tag{2.38}$$

with $\mu = 1$ for H-K flow and $\mu = \frac{1}{V}$ for the R-J flow.

Finally, we remark that the existence and the uniqueness of the two models with symmetrical obstacles were studied by J. Serrin [5].

§3 THE NUMERICAL IMPLEMENTATIONS

The integral equations (2.14) and (2.28) are solved numerically using successive iterations

$$l_{k+1}(s) = F[l_k(s);\ \Psi(l_k(s)), {S_0}^k], \tag{3.1}$$

$$l_{k+1}(s) = G[l_k(s);\ \Psi(l_k(s)), {S_0}^k, {\zeta_I}^k, {\zeta_D}^k]. \tag{3.2}$$

In what follows, we will elaborate how these iterations can be done efficiently.

We start with some features shared by both iterations. $\Omega(\zeta)$, defined by (2.6), has the property $\overline{\Omega(\zeta)} = \Omega(\bar{\zeta})$. In particular, upon analytic continuation to the boundary, one has

$$\Theta(e^{is}) = \Theta(e^{-i(2\pi - s)}), \qquad T(e^{is}) = -T(e^{-i(2\pi - s)}), \quad 0 \le s \le \pi. \tag{3.3}$$

Thus 2π-periodic extension allows $u(s) := \Theta(e^{is})$ to be represented by a Fourier series

$$u(s) = \sum_{m=-\infty}^{\infty} a_m e^{ims}, \tag{3.4}$$

with $a_{-m} = \bar{a}_m$, $m \in Z$. $T(e^{is})$ can then be found by applying conjugation operator K,

$$v(s) := T(e^{is}) = K[u](s) = -i \sum_{-\infty}^{\infty} \sigma_m a_m e^{ims} \tag{3.5}$$

where

$$\sigma_m = \begin{cases} 1 & m > 0 \\ 0 & m = 0 \\ -1 & m < 0\ . \end{cases}$$

A fast Fourier transform (FFT) is employed to implement a discrete version of these. (See [18] for more details.) We will now describe the iterations in more detail.

The Iteration for H-K Flow.

0). Make an initial guess, $l_0(s)$, for $l(s)$ at prescribed Fourier points.

Suppose kth approximation, $l_k(s)$, to $l(s)$ is known.

1). Determine

$$S_0{}^k = \frac{1}{\pi}\int_0^\pi \Psi[l_k(s)]ds$$

2). Compute $u_k(s) = \Psi[l_k(s)]$, the approximation to $u(s)$, using an FFT, with extensions made with (3.3), and calculate $v_k(s) = K[u_k](s)$, the approximation to $v(s)$, using the truncated form of (3.5).

3). Update $l_k(s)$ at Fourier points with

$$l_{k+1}(s) = 4M_k \int_0^s e^{-v_k(\theta)} \sin^2\left(\frac{\theta + S_0{}^k}{2}\right) \sin\theta d\theta,$$

where

$$M_k(s) = \frac{L}{4}\left\{\int_0^\pi e^{-v_k(s)} \sin^2\left(\frac{s + S_0{}^k}{2}\right) \sin s ds\right\}^{-1}.$$

4). If $\|l_{k+1} - l_k\|_\infty \le TOL$ (prescribed tolerance), exit with numerical boundary correspondence $l_{k+1}(s)$. Otherwise, $k \leftarrow k+1$ and goto 1).

5). Use $l_{k+1}(s)$ to compute forces and generate flow net.

The Iteration for R-J Flow.

0). Initialize the boundary correspondence with $l_0(s)$ at prescribed Fourier points, and specify free streamline velocity U ($< V := 1$) and the ratio $\frac{H}{M_1}$.

Suppose kth approximation, $l_k(s)$, to $l(s)$ is known.

1). Determine the updates of the parameters, $\zeta_D{}^k = d_k e^{i\beta_k}$, $\zeta_I{}^k = h_k e^{i\alpha_k}$, and $S_0{}^k$, with the nonlinear system (2.23)-(2.25) (five real equations) using $l_k(s)$.

2). Compute, using FFT, $u_k(s) = \Psi[l_k(s)]$ and $v_k(s) = K[u_k](s)$.

3). Update $l_k(s)$ at Fourier points with (see (2.26))

$$l_{k+1}(s) = \frac{M_1{}^k}{V}\int_0^s e^{-v_k(s)} \nu(s;\, S_0{}^k, \zeta_I{}^k, \zeta_D{}^k) ds,$$

where

$$M_1{}^k(s) = VL\left\{\int_0^\pi e^{-v_k(s)} \nu(s;\, S_0{}^k, \zeta_I{}^k, \zeta_D{}^k) ds\right\}^{-1}.$$

4). If $\|l_{k+1}-l_k\|_\infty \le TOL$ *(prescribed tolerance), exit with numerical boundary correspondence* $l_{k+1}(s)$*. Otherwise,* $k \leftarrow k+1$ *and goto 1).*

5). Use $l_{k+1}(s)$ *to compute forces and generate flow net.*

The following are numerical details shared by both of our algorithms. (*a*) The trivial initial guess $l_0(s) = Ls/\pi$, $s \in [0,\pi]$ is always assumed and a given obstacle is parametrized in terms of arc length l by a cubic spline. (*b*) We used the radix-2 $N = 2^M$ point *FFT* routine listed in [22]. (*c*) The compound trapezoidal formula was chosen to approximate all integrals involved with Fourier points as integration nodes. (*d*) With the converged boundary correspondence and parameters, the equivalence of (2.38),

$$z(\xi) = z_A + \mu \int_1^{\xi} e^{i\omega(\zeta)} \frac{dw}{d\zeta}\, d\zeta \quad \varepsilon \le \xi \le 1, \quad z(\xi) = z_B + \mu \int_1^{\xi} e^{i\omega(\zeta)} \frac{dw}{d\zeta}\, d\zeta \quad -1 \le \xi \le -\varepsilon$$

were used to generate the free streamlines with some small $\varepsilon > 0$, since $w'(\zeta)$ is singular at $\zeta = 0$. Although $\omega(\zeta)$ can be computed as $\Omega(\zeta)$ was using an *FFT*, the following formulae (from (2.8) and (2.19) respectively) are actually used in order to avoid using $\theta(e^{is})$, which is discontinuous (see (2.4)),

$$e^{i\omega(\zeta)} = e^{i\Omega(\zeta)} \frac{\zeta e^{iS_0} - 1}{\zeta - e^{iS_0}}, \qquad \text{(H-K model)}$$

$$e^{i\omega(\zeta)} = e^{i\Omega(\zeta)} \frac{(\zeta - \overline{\zeta}_D)(\zeta\zeta_D - 1)(\zeta e^{iS_0} - 1)}{(\zeta - \zeta_D)(\zeta\overline{\zeta}_D - 1)(\zeta - e^{iS_0})}. \qquad \text{(R-J model)}$$

The Fourier coefficients of $\Omega(\zeta)$ are available when exiting from the iteration.

For the H-K flow, we also generated streamlines and equi-potential lines for our computed examples using

$$z(w) = z_0 + \int_0^{w} e^{i\omega(\zeta(w^*))}\, dw^*, \tag{3.6}$$

with $z_0 = z(w_0)$ appropriately chosen. (3.6) maps a rectilinear grid in the w-plane conformally onto the flow net in the z-plane. $\zeta(w^*)$ is determined by the root of the equation

$$\zeta^2 - 2(\cos S_0 - \sqrt{w/M}\,)\zeta + 1 = 0$$

satisfying $|\zeta| < 1$. (since the roots ζ_1 and ζ_2 satisfy $\zeta_1\zeta_2 = 1$, the above equation has only one root in $|\zeta| < 1$.)

Consider now the R-J model. First, since direct use of (2.23) is inappropriate for

the numerical computations, The following alternative was actually used

$$e^{i\Omega(\zeta_I)}\frac{(\zeta_I-\bar{\zeta}_D)(\zeta_I\zeta_D-1)(\zeta_I e^{iS_0}-1)}{(\zeta_I-\zeta_D)(\zeta_I\bar{\zeta}_D-1)(\zeta_I-e^{iS_0})}=\frac{V}{U}. \tag{3.7}$$

Equation (2.24) can be written as

$$i\Omega'(\zeta_I)+\frac{2}{\zeta_I-e^{iS_0}}+\frac{2}{\zeta_I-\bar{\zeta}_D}+\frac{2\zeta_D}{\zeta_I\zeta_D-1}-\frac{1}{\zeta_I}-\frac{2}{\zeta_I-\bar{\zeta}_I}-\frac{2\bar{\zeta}_I}{\zeta_I\bar{\zeta}_I-1}=0, \tag{3.8}$$

and a lengthy calculation shows that equation (2.25) is equivalent to

$$\begin{aligned}Im\{&\frac{(\zeta_I-e^{iS_0})(\zeta_I-e^{-iS_0})(\zeta_I-\zeta_D)(\zeta_I-\bar{\zeta}_D)(\zeta_I\zeta_D-1)(\zeta_I\bar{\zeta}_D-1)}{\zeta_I(\zeta_I-\bar{\zeta}_I)^2(\zeta_I\bar{\zeta}_I-1)^2}[\frac{1}{\zeta_I-e^{iS_0}}+\\&\frac{1}{\zeta_I-e^{-iS_0}}+\frac{1}{\zeta_I-\zeta_D}+\frac{1}{\zeta_I-\bar{\zeta}_D}+\frac{\zeta_D}{\zeta_I\zeta_D-1}+\frac{\bar{\zeta}_D}{\zeta_I\bar{\zeta}_D-1}-\frac{1}{\zeta_I}-\frac{2}{\zeta_I-\bar{\zeta}_I}-\frac{2\bar{\zeta}_I}{\zeta_I\bar{\zeta}_I-1}]\}=\frac{H}{2\pi M_1}.\end{aligned} \tag{3.9}$$

In our actual computations, instead of specifying H, we input the ratio $\frac{H}{M_1}$. After M_1 is determined, H can be recovered. This treatment simplifies the nonlinear system considerably. The system (2.23)-(2.25) was solved by nonlinear system solver DNSQE [21]. The initial guess for the unknowns of the system only needs to be supplied once in order to carry out the first iteration. The solution of the unknowns in the previous iteration are then used as the initial guess in the next iteration. There are no specific requirements for choosing an initial guess in the first iteration except that $h<d$ and $0<\alpha,\beta<\pi$ are assumed for $\zeta_I=he^{i\alpha}$, $\zeta_D=de^{i\beta}$. (2.19) can also be used to compute the limiting direction,

$$\gamma=\omega(0)=\Theta(0)+iLog\frac{\zeta_D e^{iS_0}}{\bar{\zeta}_D}=\int_0^{\pi}\Psi[l(s)]ds-S_0-2arg(\zeta_D). \tag{3.10}$$

If the obstacle is symmetric, $S_0=\frac{\pi}{2}$, $\zeta_I=ih$, $\zeta_D=id$, and $H=0$. Equation (2.25) then disappears and the rest of the equations in the nonlinear system are simplified greatly. (The corresponding formulae can be found in [2] except for the equation (33.17), where factor $\frac{1}{2}$ is missing in the front of $\nu(s;\ b,h)$.)

Finally, the formulation of R-J model is reduced to the one for H-K model if the cavitation number $\sigma=0$. Indeed, since $\zeta_I=\zeta_D=0$, equation (2.16) is reduced to

$$w'(\zeta)=M_1\zeta^{-3}(\zeta^2-1)(\zeta-e^{iS_0})(\zeta-e^{-iS_0}),$$

and hence $\underset{\zeta=0}{Res}[w'(\zeta)]=0$. Since $z(\zeta)$ is now analytic at 0, one gets $\underset{\zeta=0}{Res}(\frac{dz}{d\zeta})=0$. One also has $\omega(0)=0$ and $U=V=1$, which imply that equations (2.23)-(2.25) are satisfied automatically. (2.26) then becomes (2.11).

§4 THE CONVERGENCE OF THE H-K ITERATION

An L_2-estimate for $l_k(s)-l(s)$ will be given in this section for the H-K iteration. We recall form of the iteration,

$$l_{k+1}(s)=4M_k\int_0^s e^{-K[\Psi(l_k)](\theta)}\sin^2(\frac{\theta+S_0{}^k}{2})\,\sin\theta d\theta \tag{4.1}$$

where

$$M_k=\frac{L}{4}\{\int_0^\pi e^{-K[\Psi(l_k)](s)}\sin^2(\frac{s+S_0{}^k}{2})\,\sin s ds\}^{-1}, \tag{4.2}$$

and

$$S_0{}^k=\Theta(0)=\frac{1}{\pi}\int_0^\pi \Psi[l_k(s)]\,ds. \tag{4.3}$$

Without loss of generality, we may assume $0\le l_k(s)\le L$ for all k. We need two lemmas for the proof of our theorem.

Lemma 4.1 *Assume that $l_k(s)$, defined by (4.1), satisfies a Lipschitz condition with a constant independent of k and the curvature of the obstacle, $\kappa(l)$ is continuous. Then*

$$\|K[\Psi(l_k)](s)\|_{C[0,\pi]}\le \pi L_p \underset{0\le l\le L}{Sup}\{\kappa(l)\}:=C_{LK}, \tag{4.4}$$

where L_p is the uniform Lipschitz constant.

PROOF: As a consequence of the Poisson representation for $\Omega(\zeta,l_k)$ [2], we have

$$K[\Psi(l_k)](s)=Im\{\Omega(e^{is},l_k)\}=\frac{\sin s}{\pi}\int_0^\pi \frac{\Psi[l_k(s')]-\Psi[l_k(s)]}{\cos s'-\cos s}ds'$$

$$=\frac{\sin s}{\pi}\int_0^\pi \frac{\Psi[l_k(s')]-\Psi[l_k(s)]}{l_k(s')-l_k(s)}\,\frac{l_k(s')-l_k(s)}{s'-s}\,\frac{s'-s}{\cos s'-\cos s}\,ds'. \tag{4.5}$$

It can be shown that $\sin s\frac{s'-s}{\cos s'-\cos s}$ is bounded by π for $s',s\in[0,\pi]$. From (4.5), one then easily obtains (4.4). □

Note *The estimate (4.4) is also valid for the exact boundary correspondence $l(s)$ if L_p is a Lipschitz constant for $l(s)$.*

Lemma 4.2 *Let $f(z)$ be analytic in the unit disk and real on the real axis. Suppose f can be continuously extended to the boundary and $u := Re[f(e^{is})]$. Then*

$$\| K[u] \|_{L_2[0,\pi]} \leq \| u \|_{L_2[0,\pi]}. \tag{4.6}$$

PROOF: Denote $f(e^{is}) = u(s) + iv(s)$ with $v(s) = K[u](s)$, and consider the integral

$$I := \frac{1}{i} \int_{|z|=1, Imz \geq 0} \frac{[f^+(z)]^2}{z}\, dz,$$

where $f^+(z)$ denotes the function that extends $f(z)$ to the boundary. Then

$$I = \int_0^\pi [u(s) + iv(s)]^2 ds = \int_0^\pi u^2(s) ds - \int_0^\pi v^2(s) ds + 2i \int_0^\pi u(s) v(s) ds. \tag{4.7}$$

Let Γ_1 be the upper half circle AB, Γ_2 the path $BCDA$, and write $\Gamma = \Gamma_1 \cup \Gamma_2$ (see Figure 4), where $C = -\varepsilon$ and $D = \varepsilon$. We then have

$$I = \frac{1}{i} \oint_\Gamma \frac{[f^+(z)]^2}{z}\, dz - \frac{1}{i} \int_{\Gamma_2} \frac{[f^+(z)]^2}{z}\, dz.$$

The first integral is zero due to the analyticity of the integrand. Therefore

$$\begin{aligned} I = -\frac{1}{i} \int_{\Gamma_2} \frac{[f(z)]^2}{z} dz &= -\frac{1}{i} \int_{-1}^{-\varepsilon} \frac{[f(t)]^2}{t}\, dt - \frac{1}{i} \int_\pi^0 \frac{[f(\varepsilon e^{i\theta})]^2}{\varepsilon e^{i\theta}}\, d(\varepsilon e^{i\theta}) - \frac{1}{i} \int_\varepsilon^1 \frac{[f(t)]^2}{t}\, dt \\ &= \frac{1}{i} \int_\varepsilon^1 \frac{[f(-t)]^2 - [f(t)]^2}{t}\, dt + i \int_0^\pi [f(\varepsilon e^{i\theta})]^2 d\theta. \end{aligned}$$

Letting $\varepsilon \to 0$, we obtain

$$I = \pi [f(0)]^2 - i \int_0^1 \frac{[f(-t)]^2 - [f(t)]^2}{t}\, dt. \tag{4.8}$$

Since f is real on the real axis,

$$\int_0^\pi u^2(s) ds - \int_0^\pi v^2(s) ds = \pi [f(0)]^2 \geq 0. \qquad \square$$

Theorem 4.1 *Let $l_k(s)$ be defined by the iteration procedure (4.1)-(4.3), and let all assumptions of Lemma 4.1 be satisfied. Then the following estimate holds*

$$\| l_{k+1} - l \|_{L_2[0,\pi]} \le C(\Psi) \sup_{0 \le l \le L} \{\kappa(l)\} \| l_k - l \|_{L_2[0,\pi]}, \tag{4.9}$$

where $$C(\Psi) = \pi L(\frac{1}{\sqrt{2}} + \frac{1}{2\sqrt{3}}) e^{2C_{LK}} + 4\pi(1+\pi) M \frac{1}{\sqrt{3}} e^{3C_{LK}}.$$

PROOF: From (4.1)-(4.3), (2.9), (2.12), and (2.13), one has

$$l_{k+1}(s) - l(s) = 4M_k D_1(s) + 4(M_k - M) D_2(s), \tag{4.10}$$

where

$$D_1(s) = \int_0^s e^{-K[\Psi(l_k)](\theta)} \sin^2(\frac{\theta + S_0{}^k}{2}) \sin\theta d\theta - \int_0^s e^{-K[\Psi(l)](\theta)} \sin^2(\frac{\theta + S_0}{2}) \sin\theta d\theta \tag{4.11}$$

and

$$D_2(s) = \int_0^s e^{-K[\Psi(l)](\theta)} \sin^2(\frac{\theta + S_0}{2}) \sin\theta d\theta. \tag{4.12}$$

From lemma 4.1,

$$\| D_2 \|_{L_2} = \{ \int_0^\pi \left| \int_0^s e^{-K[\Psi(l)](\theta)} \sin^2(\frac{\theta + S_0}{2}) \sin\theta d\theta \right|^2 ds \}^{\frac{1}{2}}$$

$$\le e^{C_{LK}} (\int_0^\pi s^2 ds)^{\frac{1}{2}} = \frac{\pi^{\frac{3}{2}} e^{C_{LK}}}{\sqrt{3}}. \tag{4.13}$$

$D_1(s)$ can be estimated as follows. First, we write $D_1(s)$ as

$$D_1(s) = \int_0^s g(\theta) h(\theta) d\theta + \int_0^s p(\theta) q(\theta) d\theta, \tag{4.14}$$

where

$$g(\theta) := e^{-K[\Psi(l_k)](\theta)} \sin\theta, \quad h(\theta) := \sin^2(\frac{\theta + S_0{}^k}{2}) - \sin^2(\frac{\theta + S_0}{2}),$$

$$p(\theta) := e^{-K[\Psi(l_k)](\theta)} - e^{-K[\Psi(l)](\theta)}, \quad q(\theta) := \sin\theta \sin^2(\frac{\theta + S_0}{2}).$$

Then

$$\| D_1 \|_{L_2} \le \{ \int_0^\pi [\int_0^s | g(\theta) h(\theta) | d\theta]^2 ds \}^{\frac{1}{2}} + \{ \int_0^\pi [\int_0^s | p(\theta) q(\theta) | d\theta]^2 ds \}^{\frac{1}{2}}$$

$$\le [\int_0^\pi (\int_0^s | g(\theta) |^2 d\theta) (\int_0^s | h(\theta) |^2 d\theta) ds]^{\frac{1}{2}} + [\int_0^\pi (\int_0^s | p(\theta) |^2 d\theta) (\int_0^s | q(\theta) |^2 d\theta) ds]^{\frac{1}{2}}$$

$$= H_1 + H_2. \tag{4.15}$$

Mean-value theorem implies

$$\int_0^s | h(\theta) |^2 d\theta = \le \frac{s}{4} \left| S_0{}^k - S_0 \right|^2. \tag{4.16}$$

The *RHS* of (4.16) can be estimated by (using (2.9), (4.3), the Cauchy-Schwarz inequality, and mean-value theorem)

$$\left|S_0{}^k - S_0\right|^2 \le \frac{1}{\pi^2}\{\int_0^\pi \Psi[l_k(s)] - \Psi[l(s)]ds\}^2$$

$$\le \frac{1}{\pi^2}\sup_{0\le l\le L}\{\kappa^2(l)\}(\int_0^\pi |l_k(s)-l(s)|ds)^2$$

$$\le \frac{1}{\pi}\sup_{0\le l\le L}\{\kappa^2(l)\}\,\|l_k - l\|_{L_2}^2. \tag{4.17}$$

By Lemma 4.1,

$$\int_0^s |g(\theta)|^2 d\theta \le s e^{2C_{LK}}. \tag{4.18}$$

From (4.17) and (4.18),

$$H_1 \le [\frac{e^{2C_{LK}}}{4\pi}\sup_{0\le l\le L}\{\kappa^2(l)\}\,\|l_k - l\|_{L_2}^2\int_0^\pi s^2 ds]^{\frac{1}{2}}$$

$$= \frac{\pi e^{C_{LK}}}{2\sqrt{3}}\sup_{0\le l\le L}\{\kappa(l)\}\,\|l_k - l\|_{L_2}. \tag{4.19}$$

To estimate H_2, note first

$$\int_0^s |q(\theta)|^2 d\theta \le s$$

and

$$H_2 \le \|p\|_{L_2}(\int_0^\pi s ds)^{\frac{1}{2}} = \|p\|_{L_2}\frac{\pi}{\sqrt{2}}.$$

Therefore, Lemma 4.2, together with mean-value theorem, gives

$$\|p\|_{L_2} \le e^{C_{LK}}\|K[\Psi(l_k)] - K[\Psi(l)]\|_{L_2} = e^{C_{LK}}\|K[\Psi(l_k) - \Psi(l)]\|_{L_2}$$

$$\le e^{C_{LK}}\|\Psi(l_k) - \Psi(l)\|_{L_2} \le e^{C_{LK}}\sup_{0\le l\le L}\{\kappa(l)\}\,\|l_k - l\|_{L_2},$$

hence

$$H_2 \le \frac{\pi}{\sqrt{2}}e^{C_{LK}}\sup_{0\le l\le L}\{\kappa(l)\}\,\|l_k - l\|_{L_2}. \tag{4.20}$$

Combining the results stated by (4.15), (4.19), and (4.20),

$$\|D_1\|_{L_2} \le \pi(\frac{1}{\sqrt{2}} + \frac{1}{2\sqrt{3}})e^{C_{LK}}\sup_{0\le l\le L}\{\kappa(l)\}\,\|l_k - l\|_{L_2}. \tag{4.21}$$

The estimate for $|M_k - M|$ can be carried out as follows. First,

$$|M_k - M| = \frac{L}{4} \frac{D_1(\pi)}{\{\int_0^\pi e^{-K[\Psi(l_k)](\theta)} \sin^2(\frac{\theta + S_0{}^k}{2}) \sin\theta d\theta\}\{\int_0^\pi e^{-K[\Psi(l)](\theta)} \sin^2(\frac{\theta + S_0}{2}) \sin\theta d\theta\}},$$

and, since

$$\int_0^\pi e^{-K[\Psi(l)](\theta)} \sin^2(\frac{\theta + S_0}{2}) \sin\theta d\theta = \frac{L}{4M}$$

and

$$2\int_0^\pi \sin^2(\frac{\theta + S_0{}^k}{2}) \sin\theta d\theta = \int_0^\pi [1 - \cos(\theta + S_0{}^k)] \sin\theta d\theta = 2 + \frac{\pi}{2} \sin S_0{}^k, \tag{4.22}$$

one gets

$$|M_k - M| \le \frac{M e^{C_{LK}}}{1 + \frac{\pi}{4} \sin S_0{}^k} |D_1(\pi)|. \tag{4.23}$$

By essentially the same fashion as in estimating $\|D_1\|_{L_2}$, one has

$$\begin{aligned}
|D_1(\pi)| &\le \int_0^\pi g(\theta) |h(\theta)| d\theta + \int_0^\pi |p(\theta)| q(\theta) d\theta \\
&\le e^{C_{LK}} |S_0{}^k - S_0| \int_0^\pi \sin\theta d\theta + e^{C_{LK}} \int_0^\pi |K[\Psi(l_k) - \Psi(l)](\theta)| d\theta \\
&\le 2e^{C_{LK}} |S_0{}^k - S_0| + e^{C_{LK}} (\int_0^\pi 1^2 d\theta)^{\frac{1}{2}} (\int_0^\pi |K[\Psi(l_k) - \Psi(l)](\theta)|^2 d\theta)^{\frac{1}{2}} \\
&\le \frac{2e^{C_{LK}}}{\sqrt{\pi}} \sup_{0 \le l \le L} \{\kappa(l)\} \|l_k - l\|_{L_2} + \sqrt{\pi} e^{C_{LK}} \sup_{0 \le l \le L} \{\kappa(l)\} \|l_k - l\|_{L_2} \\
&\le \frac{(2+\pi) e^{C_{LK}}}{\sqrt{\pi}} \sup_{0 \le l \le L} \{\kappa(l)\} \|l_k - l\|_{L_2}.
\end{aligned} \tag{4.24}$$

One then obtains from (4.23), and (4.24)

$$|M_k - M| \le \frac{(2+\pi) M e^{C_{LK}}}{\pi^{\frac{1}{2}} (1 + \frac{\pi}{4} \sin S_0{}^k)} \sup_{0 \le l \le L} \{\kappa(l)\} \|l_k - l\|_{L_2}. \tag{4.25}$$

Using (4.22), one also has

$$|M_k| \le \frac{L e^{C_{LK}}}{4(1 + \frac{\pi}{4} \sin S_0{}^k)}. \tag{4.26}$$

Combining all of the above and assuming, without loss of generality, $0 \le S_0{}^k \le \pi$, one finally gets

$$\|l_{k+1} - l\|_{L_2} \le 4 |M_k| \|D_1\|_{L_2} + 4 |M_k - M| \|D_2\|_{L_2}$$

$$\leq \pi L e^{2C_{LK}}\left(\frac{1}{\sqrt{2}}+\frac{1}{2\sqrt{3}}\right) \sup_{0\leq l\leq L}\{\kappa(l)\}\,\|l_k-l\|_{L_2}\cdot$$

$$+4M\pi(2+\pi)\frac{1}{\sqrt{3}}\,e^{3C_{LK}} \sup_{0\leq l\leq L}\{\kappa(l)\}\,\|l_k-l\|_{L_2}\cdot$$

$$\leq C(\Psi) \sup_{0\leq l\leq L}\{\kappa(l)\}\,\|l_k-l\|_{L_2}. \qquad \square$$

Corollary 4.1 *Under the assumptions of Theorem 4.1, if, in addition, the obstacle is such that*

$$C(\Psi) \sup_{0\leq l\leq L}\{\kappa(l)\} < 1, \tag{4.27}$$

the H-K iteration is linearly convergent.

Remark *Theorem 4.1 is in the character of an a posteriori estimate, and can only be used to guarantee convergence if an a priori estimate for the Lipschitz constants of l_k can be obtained and the curvature satisfies an appropriate inequality. Nevertheless it has interesting relations with the examples reported in the next section.*

§5 COMPUTED EXAMPLES

In this section some numerical results are presented for both models. In addition to the notations used before, we will use the following abbreviations: *NFP* (the number of Fourier points), *NIT* (the number of iterations), $C_D = X/(\frac{1}{2}\rho U^2 S)$ (drag coefficients, where X being the drag force, U being the flow velocity at infinity, and S being the projected area of the obstacle perpenticular to the stream), C_L (lift coefficient defined similarly with Y, the lift force), $SER := \|l_{k+1}-l_k\|_\infty$ (successive iteration error). Two Fortran programs called TIMKIRCH and NRJET were written to implement all reported computations. All computations were done on an IBM *ES*9121 Model 440 was used on at Wichita State University in double precision arithmetic. We start with examples for the H-K flow.

1. FLAT PLATE. The vertical flat plates (Figure 5(*a*)) was treated by many authors. An analytic solution is available, if $L=1$, $C_D = 2\pi/(4+\pi)$. Our results show that 2^8 Fourier points gives results accurate up to 4 decimal digits. Figure 5(*b*) and

Figure 5(c) are flows past plates with angle of attack 30^0 and 60^0 respectively. The exact values of C_D and C_L up to five decimal places are available in, *e.g.*, [6]. The solution always converged in two iterations with $SER = 0.1E\text{-}15$. The conclusion of Theorem 4.1 explains why this happened, since the curvature of a plate is zero everywhere. (The efficiency of the method reported in [6] should be compared for these examples.)

For these flat plate problems the accuracy of the results is solely dominated by the number of Fourier points used in the computation. In general, it seems true from our numerical experiments that SER always does to (machine) zero if NIT is big enough as long as SER is decreasing in the first few iterations. Therefore, the numerical results can be made as accurate as desired by increasing NFP if the iteration is convergent.

2. SYMMETRIC CIRCULAR ARC. This is also a classic example and some numerical results were reported in [1]. With break-away angle 55^0, $NFP = 2^{10}$ and $NIT = 10$, we have $SER = 0.2E\text{-}6$ and $C_D = 0.49859$ (results in [6] should be compared here). Figure 6 shows the arc with break-away angle 45^0. This example was also used to show two strategies that we used to accelerate the convergence. One of them is under-relaxation process defined by

$$l_{k+1}(s) = (1-\varepsilon) l_k(s) + \varepsilon \widetilde{P}\,[l_k](s), \tag{5.1}$$

where $\widetilde{P}$ is the iteration operator without relaxation and ε $(0 < \varepsilon < 1)$ is the relaxation factor, chosen by trial and error. The other is Aitken's Δ^2 acceleration [20], which is suitable for any linearly convergent sequence. If l_k is the original sequence, the new one, which accelerates the convergence of l_k, is defined by

$$l^{new}_{k+1} = l_{k+1} - \frac{(l_{k+1} - l_k)^2}{l_{k+1} - 2l_k + l_{k-1}}. \tag{5.2}$$

The numerical results for this example are presented in the following table, for which $NFP = 2^{10}$.

	NIT	*SER of the iteration*
original sequence l_k	10	$0.14 \times E-6$
relaxation with $\varepsilon = 0.89$	5	$0.66 \times E-5$
Aitken's Δ^2 *method*	6	$0.64 \times E-6$

3. AN ASYMMETRIC WEDGE. This is a plate $(L = 1)$ bent at the middle with

lower half inclined at 45^0 and upper half at 30^0 (see Figure 7). The problem can not be solved analytically and the numerical result was reported in [7]. The curvature of the obstacle is discontinuous at the vertex. In our computation, the obstacle is interpolated by a cubic spline. The vertex will be "smooth out" but with large curvature occurring near the vertex. A relaxation factor $\varepsilon = 0.2$ was used to improve the behavior of convergence. With $NFP = 2^{10}$ and $NIT = 50$, we got $SER = 0.26 \times E\text{-}06$, $C_D = 0.3369$ (exact: 0.3370), and $C_L = 0.0738$ (exact: 0.0739).

4. SINE CURVE. The parameter form of the curve is given by

$$x = \alpha \sin[\pi(1-2t)], \quad y = 2t - 1 \quad t \in [0,1].$$

The curvature of the curve is controlled by parameter α. Figure 8 gives three cases corresponding to different α and angle of attack. We are interested in how the curvature affects the number of iterations needed.

5. NACA 23024 AIRFOIL. The airfoil (Figure 9) is inclined at 30^0 or 15^0 angle of attack and the separation is assumed at the trailing edge and near the leading edge. A relaxation factor $\varepsilon = 0.2$ was used. (Similar examples reported in [6] should be compared here.) To achieve an accuracy of $SER = 0.1E\text{-}5$, the typical computational time for these airfoil problems, using 2^{10} Fourier points, a relaxation factor and running 50 iterations, is about 4 *CPU* seconds without plotting.

The next four examples are for re-entrant jet flows. Unfortunately, there have been almost no documented numerical results for comparison. Only the obstacles and free streamlines are shown in the plots presented.

6. FLAT PLATE. Two cases are presented in Figure 10 with angle of attack at 10^0 ($NFP = 2^8$, $V = 0.5$, $H = 0.12$) and 30^0 ($NFP = 2^8$, $V = 0.6$, $H = 0.08$), respectively. In general, the direction of the lift force experienced by the obstacle depends on strength of the circulation and the inclination of the obstacle. Again, for a flat plate, whether it is inclined or not, the method converged with $SER = E\text{-}15$ in three iterations, which strongly suggests that a similar theorem to Theorem 4.1 may exist for R-J model.

Some theoretical results available in [1] can be used here for checking our numerical results. In particular, for a vertical plate we have $\zeta_I = ic$ and $\zeta_D = ih$ with $h \le c \le BV := (1+\sqrt{5}-\sqrt{2+2\sqrt{5}}\ )/2 \approx 0.346014339$. By taking the cavitation number $\sigma = 9999999999$, we computed (with $NFP = 2^{10}$) $\zeta_I = 0.34601i$ and $\zeta_D = 0.34599i$, which

indicates, though not stated in [1], that $\lim_{\sigma\to\infty} c = \lim_{\sigma\to\infty} h = BV$. On the other hand, we also verified numerically that as $\sigma\to 0$, the flow pattern approximates that of H-K flow.

7. SINE CURVE. The parametric expression of the curve is as in the example 4. Again, we investigated how the curvature of the obstacle affects the convergence. For all the examples, $NFP = 2^8$ was used. Figure 11(a): $\alpha = \frac{1}{8}$, angle of attack $= 30^0$, $NIT = 25$, $\varepsilon = 0.9$, $V = 0.6$, $H = 0.1979$, $SER = 0.4E$-8. Figure 11(b): $\alpha = 0.3$, angle of attack $= 60^0$, $NIT = 30$, $\varepsilon = 0.6$, $V = 0.6$, $H = 0.1456$, $SER = 0.5E$-5. Figure 11(c): $\alpha = 0.5$, angle of attack $= 120^0$, $NIT = 50$, $\varepsilon = 0.6$, $V = 0.6$, $H = 0.2208$, $SER = 0.2E$-4.

8. AN ASYMMETRICAL WEDGE. The obstacle was treated in the example 3. The results correspond to Figure 12 are as follows: $NFP = 2^{10}$, $NIT = 50$, $\varepsilon = 0.2$, $V = 0.5$, $H = 0.1219$, $SER = 0.4E$-6.

9. NACA 23024 AIRFOIL. We present two cases (Figure 13) corresponding to angle of attack 30^0 and different cavitation numbers. The separation points are the same as mentioned in the example 5. With $\varepsilon = 0.2$, and $NIT = 50$, we got approximately $SER = E$-5 for both of these two examples. The computational time with $NFP = 2^{10}$ and 50 iterations is about 10 *CPU* seconds excluding plotting.

ACKNOWLEDGEMENTS

The research of the first author was partially supported by National Science Foundation grant *OSR*-9255223 under the NSF EPSCOR Program and by U.S. Department of Energy grant *DE-FG*02-92*ER*25124. The research of the second and the third authors was partially supported by National Science Foundation grant *OSR*-9255223 under the NSF EPSCOR Program.

THE CAPTION OF FIGURES

Figure 1. Flow plane (z-plane): (a) Kirchhoff flow, (b) Reentrant jets.

Figure 2. w-plane and ζ-plane of the H-K flow.

Figure 3. w-plane and ζ-plane of the R-J flow.

Figure 4. Path used in the proof of Lemma 4.2.

Figure 5. H-K flow past a flat plate.

Figure 6. H-K flow past a circular arc with break-away angle 45^0.

Figure 7. H-K flow past an asymmetrical wedge.

Figure 8. H-K flow past a sine curve.

Figure 9. H-K flow past an inclined airfoil with fixed separation points.

Figure 10. R-J flow past a flat plate.

Figure 11. R-J flow past a sine curve.

Figure 12. R-J flow past an asymmetrical wedge.

Figure 13. R-J flow past an inclined airfoil with fixed separation points.

REFERENCES

[1] G. Birkhoff & E. H. Zarantonello, *Jets, Wakes, and Cavities*, Academic Press, NewYork, 1957.

[2] D. Gilbarg, *Jet and Cavities*, Handbuch der Physik 9 , Springer, Berlin, 311-445, 1966.

[3] M. I. Gurevich, *The Theory of Jets in an Ideal Fluid*, Pergamon Press Ltd., 1966

[4] D. Gilbarg & J. Serrin, *Free boundaries and jets in the theory of cavitation*, J. Math. Phys. 29, 1-12 (1950).

[5] J. Serrin, *Existence theorems for some hydrodynamical free boundary problems*, J. Rat. Mech. Analysis, 1-48 (1952).

[6] P. J. Heink & R. T. Davis, *A conformal mapping technique for non-symmetric flows with free-streamlines*, AIAA paper, 87-98.

[7] A. R. Elcrat & L. N. Trefethen, *Classical free streamline flow over a polygonal obstacle*, J. Comput. Appl. Math. 14, 251-265 (1986).

[8] F. Dias, A. R. Elcrat, & L. N. Trefethen, *Ideal jet flow in two dimensions*, J. Fluid Mech. 185, 275-288 (1987).

[9] F. Dias & A. R. Elcrat, *Ideal jet flow with a stagnation streamline*, Eur. J. Mech. B, 11, 223-247 (1992).

[10] D. Gilbarg, *A generalization of the Schwarz-Christoffel Transformation*, Proc. Nat. Acad. Sci., 35, 609-612 (1949).

[11] P. Bassanini & A. R. Elcrat, *Free stream–boundary layer analysis for separated flow over an airfoil*, ZAMP 44, 695-706 (1993).

[12] W. W. H. Yeung & G. V. Parkinson, *A wake singularity potential flow model for airfoils expriencing trailing-edge stall*, J. Fluid Mech. 251, 203-218 (1993).

[13] J. A. Robertson, *Hydrodynamics in Theory and Application*, Prentice-Hall, Englewood Cliffs, NJ, 1965.

[14] M. Tulin, *Supercavitating flows-small perturbation theory*, J. Ship Res. 7, 16-37 (1964).

[15] T. K. DeLillo & A. R. Elcrat, *A comparison on some numerical conformal mappings for exterior regions*, SIAM J. Sci. Stat. Comput. 12, 399-422 (1991).

[16] T.K. DeLillo & A. R. Elcrat, *Numerical conformal mapping methods for exterior regions with corners*, J. Comput. Phys., Vol. 108, No. 2, 199-208 (1993).

[17] L. C. Woods, *The Theory of Subsonic Plane Flow, University Press*, Cambridge, 1961.

[18] P. Henrici, *Fast Fourier methods in computational complex analysis*, SIAM Rev., Vol. 21, No. 4, 481-527 (1979).

[19] P. Henrici, *Applied and Computational Complex Analysis*, Vol. III, John Wiley, New York, 1986.

[20] K. E. Atkinson, *An Introduction to Numerical Analysis*, John Wiley, New York, 1978.

[21] D. Kahaner, C. Moler & S. Nash, *Numerical Methods*, Prentice Hall, Englewood Cliffs, NJ, 1989, p. 258.

[22] G. Dahlquist & A. Björck, *Numerical Methods*, Prentice-Hall, Englewood Cliffs, NJ, 1974, p. 416.

ABSTRACT

Numerical algorithms are presented for two classical free boundary problems for ideal flow past an obstacle: Helmholtz-Kirchhoff and reentrant jet flows. The Levi-Civita representation of the log-hodograph function is used in each case to derive nonlinear integral equation for the boundary correspondence between the obstacle and the parameter domain. The integral equations are solved by a method of successive conjugation implemented with the fast Fourier transform. For the reentrant jet flow an additional nonlinear system must be solved to update certain flow parameters at each iteration. Several examples are computed for polygonal and curvilinear obstacles. A convergence result is given for the Helmholtz-Kirchhoff flow.

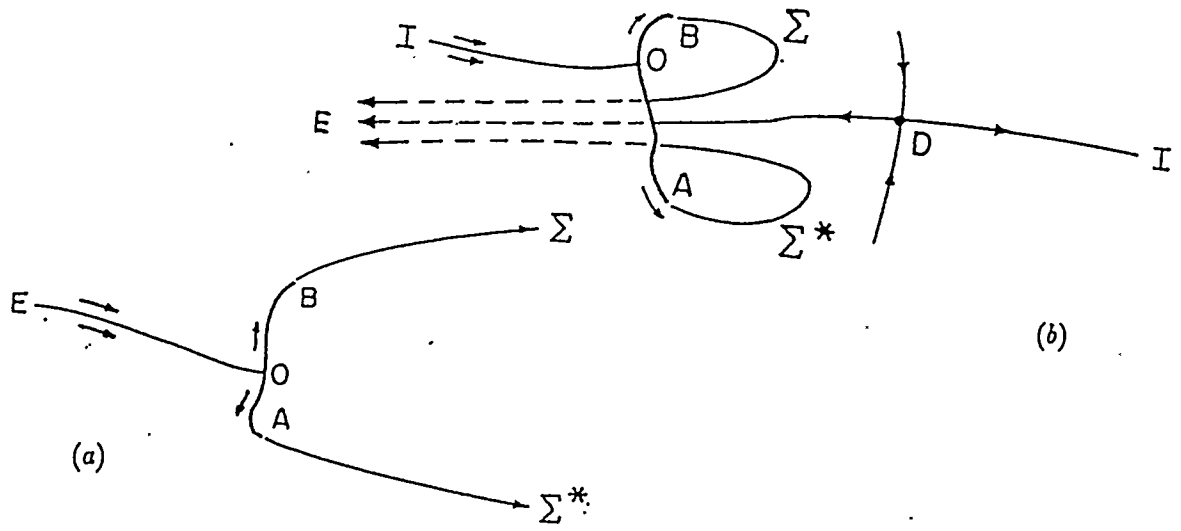

Figure 1 Flow plane (z-plane): (a) Kirchhoff flow, (b) Re-entrant jets.

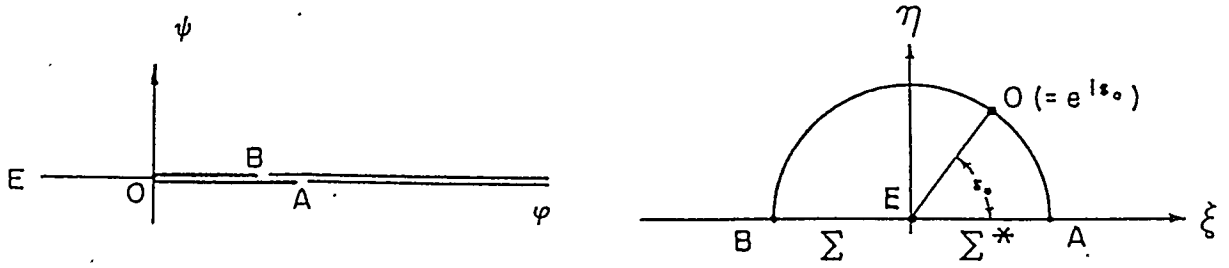

Figure 2 w-plane and ζ-plane of the H-K flow.

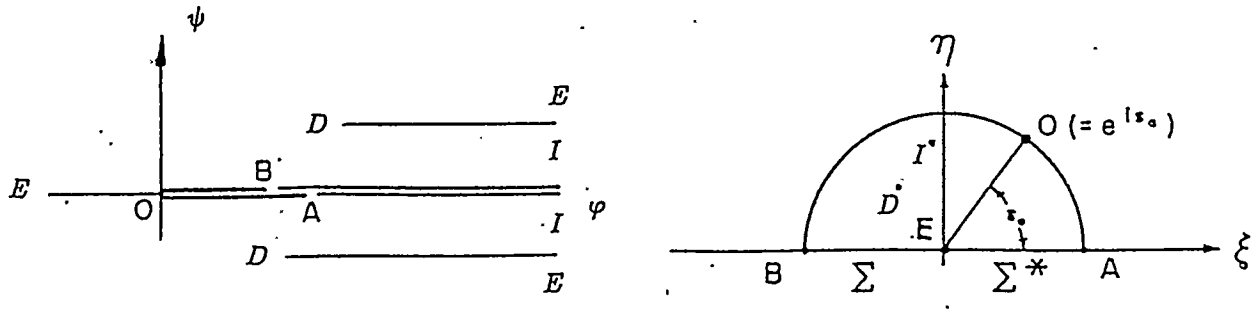

Figure 3 w-plane and ζ-plane of the R-J jet flow.

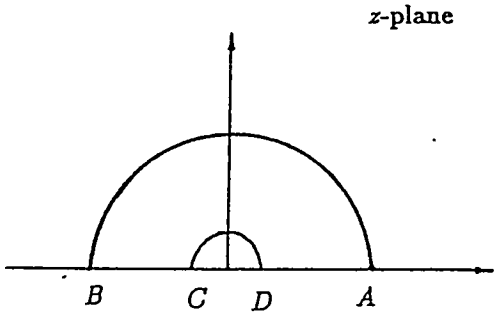

Figure 4 Path used in the proof of Lemma 4.2.

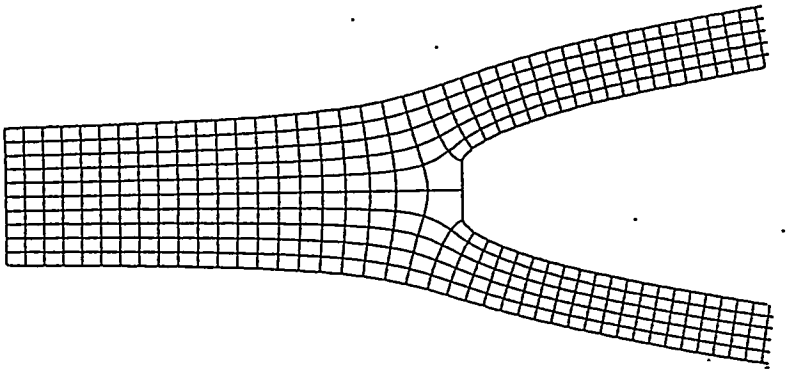

(a) $NFP = 2^{10}$, $NIT = 2$, $C_D = 0.879803$ (exact: 0.879802), $C_L = 0$.

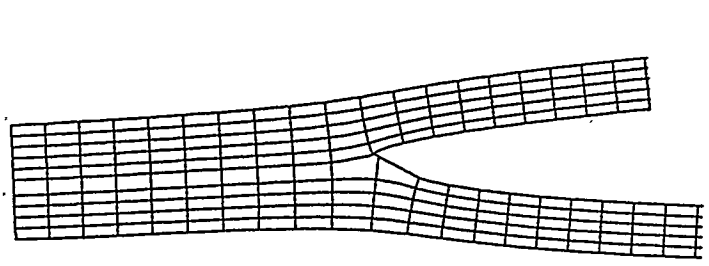

(b) $NFP = 2^{10}$, $NIT = 2$
$C_D = 0.281970$ (exact: 0.28197)
$C_L = 0.488387$ (exact: 0.48839)

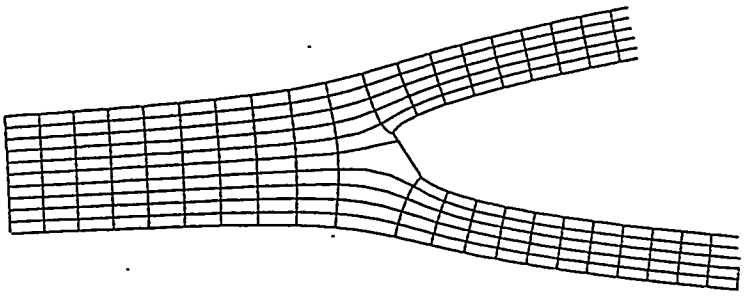

(c) $NFP = 2^{10}$, $NIT = 2$
$C_D = 0.701177$ (exact: 0.70118)
$C_L = 0.404823$ (exact: 0.40482)

Figure 5 H-K flow past a flat plate.

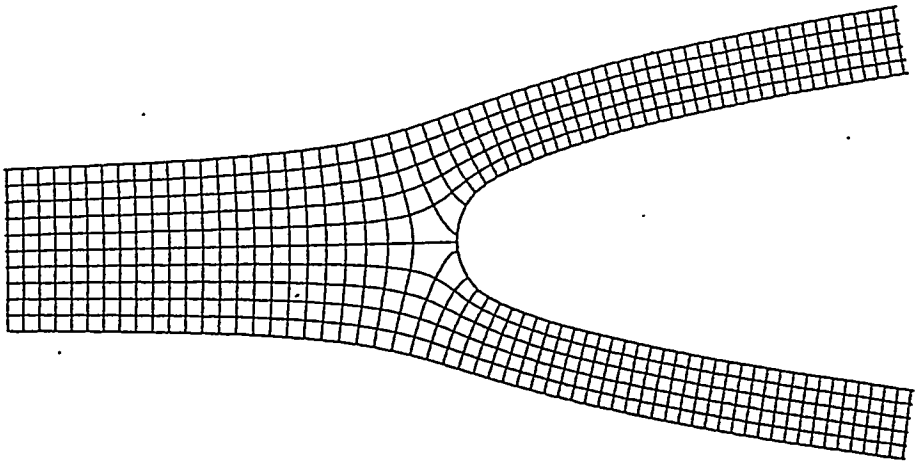

Figure 6 H-K flow past a circular arc with break-away angle 45^0.

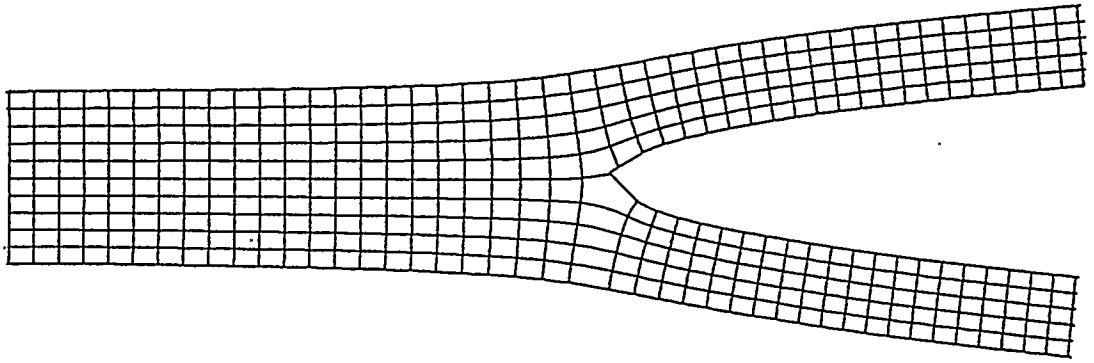

Figure 7 H-K flow past an asymmetrical wedge.

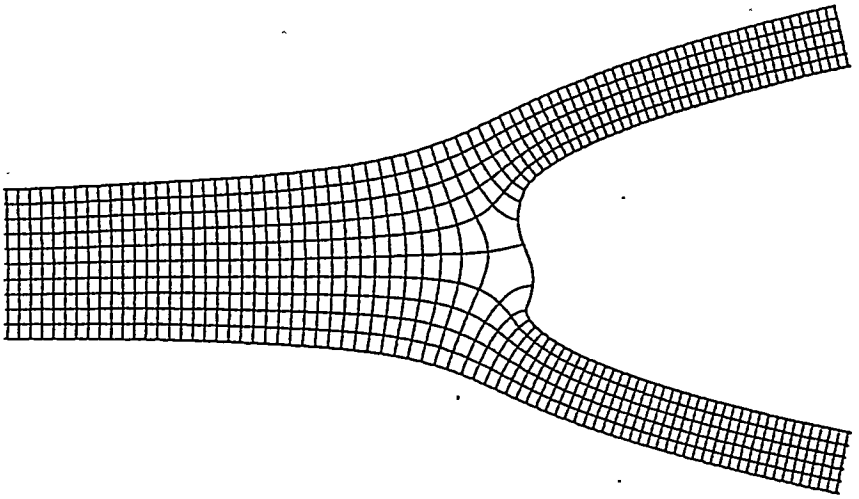

(a) $\alpha = \frac{1}{8}$, NFP $= 2^{10}$, NIT $= 20$, SER $=$ 0.1E-8.

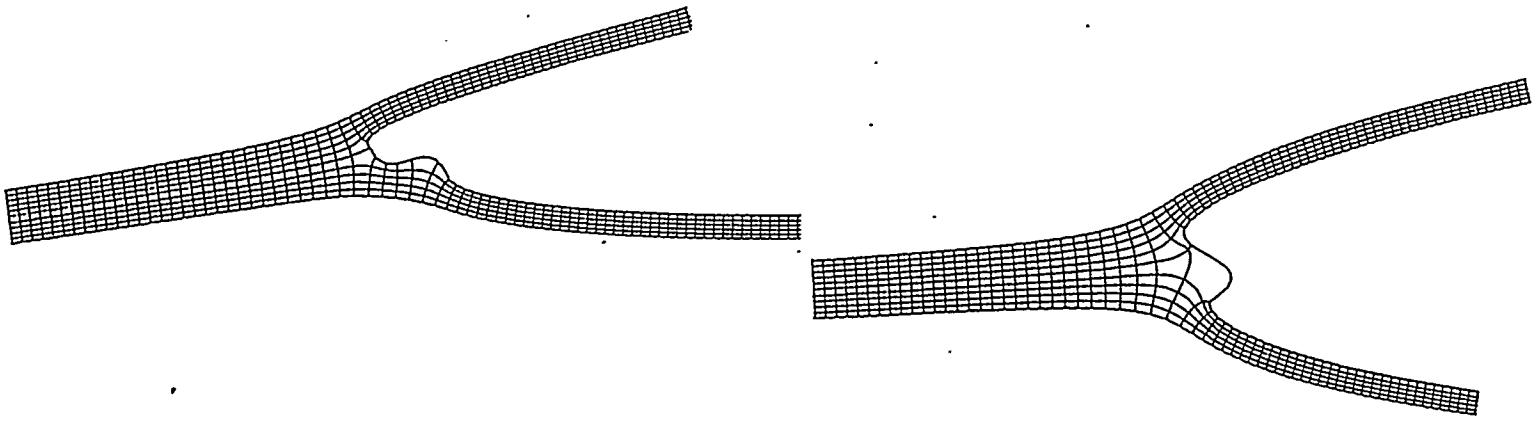

(b) $\alpha=\frac{1}{4}$, $NFP=2^{10}$, $NIT=30$, $SER=0.3E\text{-}9$. (c) $\alpha=\frac{1}{2}$, $NFP=2^{10}$, $NIT=100$, $SER=0.2E\text{-}6$.

Figure 8 H-K flow past a sine curve.

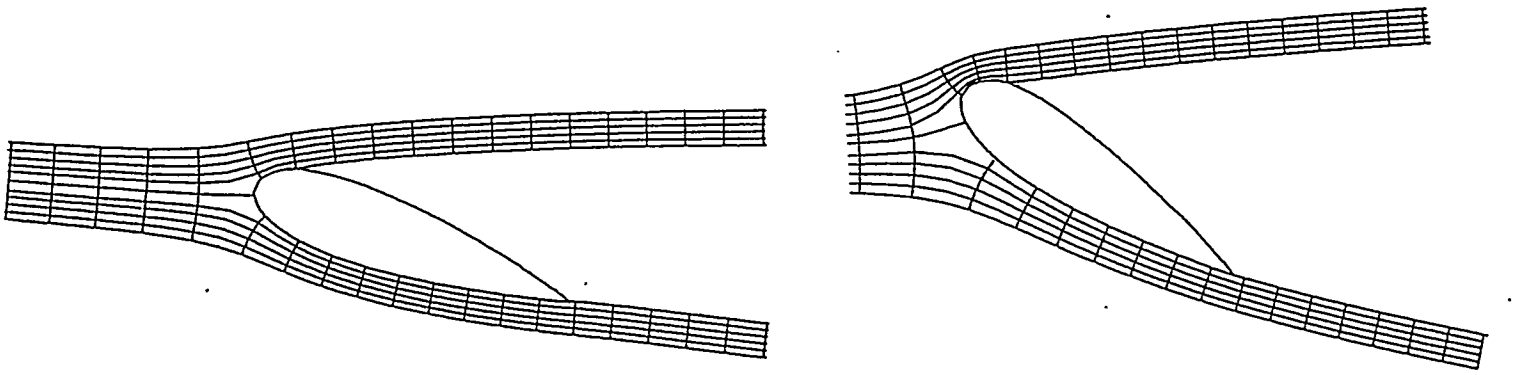

Figure 9 H-K flow past an inclined airfoil with fixed separation points.

Figure 10 R-J flow past a flat plate.

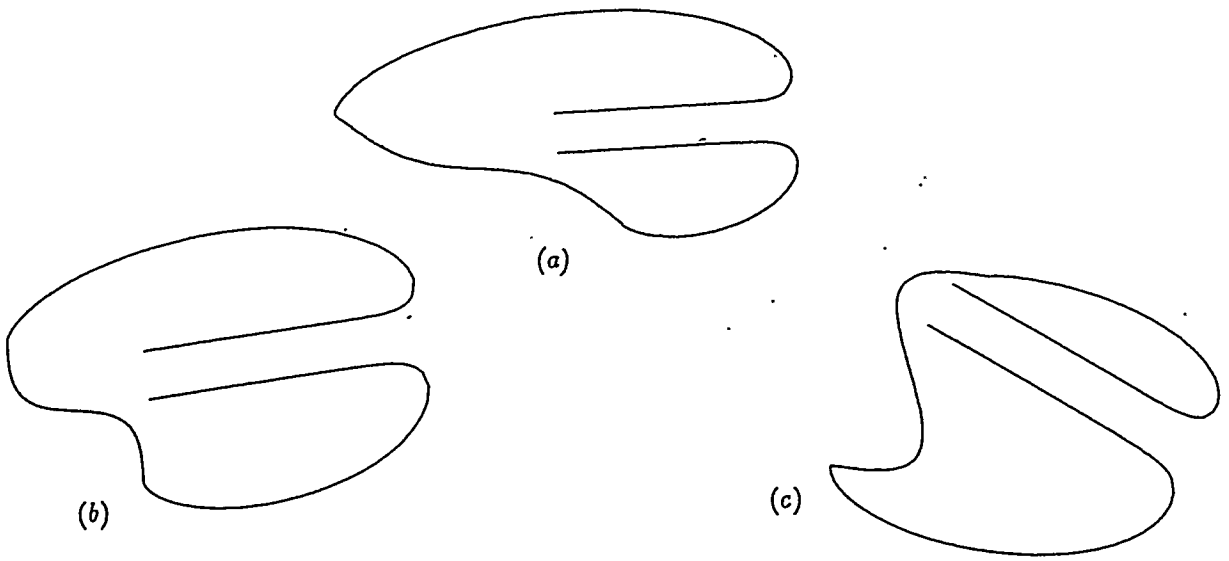

Figure 11 R-J flow past a sine curve.

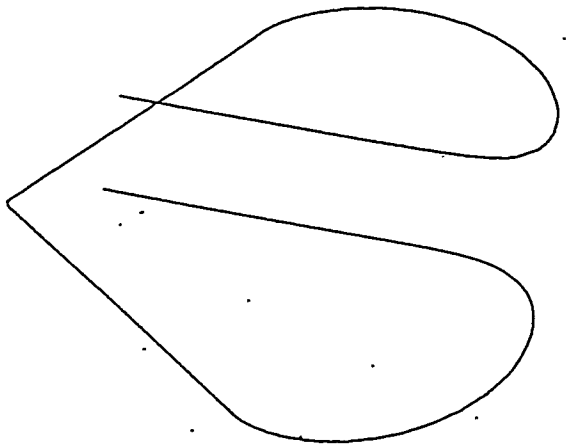

Figure 12 R-J flow past an asymmetrical wedge.

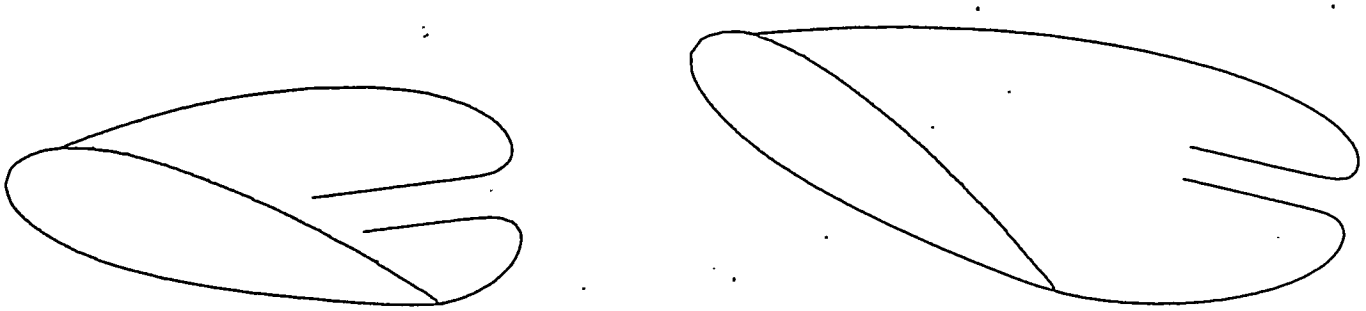

Figure 13 R-J flow past an inclined airfoil with fixed separation points.

Submitted for publication

The Numerical Solution of the Biharmonic Equation by Conformal Mapping

Raymond H. Chan¶
Department of Mathematics, The Chinese University of Hong Kong, Shatin, Hong Kong

Thomas K. DeLillo†§ and Mark A. Horn†‡,
Department of Mathematics and Statistics, Wichita State University,
Wichita, KS 67260-0033

Abstract. The solution to the biharmonic equation in a simply connected region Ω in the plane is computed in terms of the Goursat functions. The boundary conditions are conformally transplanted to the disk with a numerical conformal map. A linear system is obtained for the Taylor coefficients of the Goursat functions. The coefficient matrix of the linear system can be put in the form $I + K$ where K is the discretization of a compact operator. K can be thought of as the composition of a block Hankel matrix with a diagonal matrix. The compactness leads to clustering of eigenvalues and the Hankel structure yields a matrix-vector multiplication cost of $O(N \log N)$. Thus if the conjugate gradient method is applied to the system then superlinear convergence will be obtained. Numerical results are given to illustrate the spectrum clustering and superlinear convergence.

Key words. Biharmonic equation, numerical conformal mapping, Hankel matrices.
AMS subject classifications. 30C30, 31A30, 65E05
Abbreviated title. The Biharmonic Equation

1. Introduction. Boundary value problems for the biharmonic equation in two dimensions arise in the computation of the Airy stress function for plane stress problems [KK], [Mik], [Musk], and in steady Stokes flow of highly viscous fluids [MT, Chap. 22], [Poz]. Integral equations methods are a popular choice for the numerical solution of these equations [GGMa], [MG], [K, and references there], [Poz]. The application of conformal mapping to this problem, though classical, is less well known [KK], [Musk]. Unlike the Laplace equation, the biharmonic equation is not preserved under conformal transplantation. However, a biharmonic function and its boundary values can be represented in terms of the analytic Goursat functions and this representation can be transplanted with a conformal map to a computational region, such as a disk, an ellipse, or an annulus, where the boundary value problem can be solved more easily.

In this paper, we consider simply-connected regions with analytic boundaries and use the unit disk as our computational region. In our examples, the conformal map f from the unit disk to the region is either known explictly or approximated numerically. The

¶ This author's research was partially supported by HKRGC grant CUHK316/94E.
Email address: rchan@math.cuhk.hk

† This author's research was partially supported by U. S. Department of Energy grant DE-FG02-92ER25124 and National Science Foundation EPSCoR grant OSR-9255223.

§ Email address: delillo@twsuvm.uc.twsu.edu

‡ Email address: mhorn@twsuvm.uc.twsu.edu

boundary conditions for the biharmonic function are then transplanted by f to the disk and a linear system for the Taylor coefficients of the Goursat functions in the disk is obtained and solved efficiently by conjugate-gradient-like methods. If the boundary of the target region is smooth enough (analytic in our examples), the continuous problem can be posed as a compact operator acting on some appropriate Banach space. This will lead to a clustering of the spectrum and hence superlinear convergence.

We expect to be able to generalize this work to cases where the conformal map f is a Faber series map from an ellipse, cross-shaped or spoke-like region as in [DE] and [DEP]. If the target region has elongated sections, the conformal map from the disk may be severely ill-conditioned and an ellipse or cross-shaped region may provide a better computational region. In [GGMa] the Sherman-Lauricella equation is solved for spoke-like regions which provide difficult regions for plane stress and plane strain problems. We anticipate that our Faber series methods may have advantages for such highly distorted regions. In cases for which the target region is not too distorted, so that the map from the disk is not too severely ill-conditioned, our method may also have some advantages. For instance, if several boundary value problems have to be solved for the same region, so that the conformal map only has to be computed once, our method, which is based on the fast Fourier transform (FFT), will give accurate answers in $O(N \log N)$ for moderate sized N. The methods in [GGMa] use the fast multipole method, which costs only $O(N)$, but with a large constant, so that large N are required in practice for it to be faster than the FFT. Below, we will use the FFT-based numerical conformal mapping method given in [Weg]. Introductions to numerical conformal mapping can be found in [Ga] and [He].

The outline of the paper is as follows. In section 2, we discuss the solution of boundary value problems for the biharmonic equation in terms of Goursat functions and the conformal map from the disk to the plane region. In section 3, we discuss the special structure of the exact linear system. We will see that the coefficient matrix of the (infinite) linear system is of the form $I + HD$ where I is the identity matrix, D a diagonal matrix, and H is a block Hankel matrix. It will be seen that HD actually can be represented as a compact operator with a one dimensional null space. This system can be symmetrized and solved (up to the null vector) using the conjugate gradient method. In section 4, we formulate the discrete problem. We will show how the conjugate gradient method is applied to the discrete system and how the matrix-vector multiplication can be carried out in $O(N \log N)$. In section 5, we give several numerical examples which illustrate the spectrum clustering, the superlinear convergence, and the discretization error.

2. The biharmonic equation. Here we will follow the presentation in [KK] and [Musk]. We wish to find the Airy stress function u for a simply connected region Ω with a smooth boundary Γ in the ζ-plane. Then u satisfies the biharmonic equation,

$$\Delta^2 u = 0$$

for $\zeta = \eta + i\mu \in \Omega$. The two fundamental boundary value problems in elasticity seek to find u given the external stresses or external displacements on the boundary Γ. Both of these problems amount to specifying

$$u_\eta = G_1 \quad \text{and} \quad u_\mu = G_2$$

on Γ. The function u can be represented as

$$u(\varsigma) = Re(\overline{\varsigma}\phi(\varsigma) + \chi(\varsigma)),$$

where $\phi(\varsigma)$ and $\chi(\varsigma)$ are analytic functions in Ω known as the *Goursat functions*. Letting $G = G_1 + iG_2$, the boundary conditions for the first fundamental problem become

$$\phi(\varsigma) + \varsigma\overline{\phi'(\varsigma)} + \overline{\psi(\varsigma)} = G(\varsigma), \quad \varsigma \in \Gamma \tag{1}$$

where $\psi(\varsigma) = \chi'(\varsigma)$. The second fundamental problem leads to similar conditions. For simplicity, in this paper, we will only concentrate on the first boundary conditions (1).

We remark that $\phi(\varsigma)$ and $\psi(\varsigma)$ are not unique. In fact, if $\phi(\varsigma)$ and $\psi(\varsigma)$ represent any solution of the problem, then so does $\phi(\varsigma) + Ci\varsigma + \gamma$ and $\psi(\varsigma) + \gamma'$, where $C \in \mathbf{R}$, $\gamma \in \mathbf{C}$, and $\gamma' \in \mathbf{C}$. Thus, the constants C and γ must be specified for uniqueness of ϕ. These constants are determined below.

The problem at this point is to find ϕ and ψ analytic in Ω and satifying (1). One approach is to represent ϕ and ψ as Cauchy-type integrals of a density function on Γ. This leads to the *Sherman-Lauricella equation*, a Fredholm integral equation for the density function which can be solved efficiently by the fast multipole method [GGMa]. In this paper, we propose to solve it by using numerical conformal mapping coupled with the conjugate gradient method.

Let $\varsigma = f(z)$ be the conformal map from the unit disk to Ω, fixing $f(0) = 0 \in \Omega$. Then with $d(z) := f(z)/\overline{f'(z)}$, $\phi(z) := \phi(f(z)), \psi(z) := \psi(f(z))$, and $G(z) := G(f(z))$, equation (1) transplants to the disk as

$$\phi(z) + d(z)\overline{\phi'(z)} + \overline{\psi(z)} = G(z), \quad |z| = 1. \tag{2}$$

Let

$$\phi(z) = \sum_{k=1}^{\infty} a_k z^k \quad \text{and} \quad \psi(z) = \sum_{k=0}^{\infty} b_k z^k.$$

Notice that the sum for ϕ begins at $k = 1$. This fixes the constant γ mentioned above for uniqueness by requiring $\phi(0) = a_0 = 0$. After transplanting to the disk, the other constant is determined by setting $Im(a_1/f'(0)) = 0$.

The problem is to find the a_k's and the b_k's. For $|z| = 1$, define the Fourier series

$$d(z) := f(z)/\overline{f'(z)} = \sum_{k=-\infty}^{\infty} h_k z^k, \quad G(z) = \sum_{k=-\infty}^{\infty} A_k z^k.$$

Substituting into (2) gives a linear system of equations for the a_k's and b_k's,

$$a_j + \sum_{k=1}^{\infty} k\overline{a}_k h_{k+j-1} = A_j, \quad j = 1, 2, 3, \ldots \tag{3}$$

$$\overline{b}_j + \sum_{k=1}^{\infty} k\overline{a}_k h_{k-j-1} = A_{-j}, \quad j = 0, 1, 2, \ldots \tag{4}$$

If (3) is solved for the a_k's, then the b_k's can be easily computed from (4). Thus, in this paper, we will concentrate on an efficient method for solving (3).

There is also a moment condition to be satisfied by the data. After transplantation to the disk, this condition can be stated as $Re[\int_{|z|=1} G(z)\overline{f'(z)dz}] = 0$. This moment condition will assure the existence of a solution. Our assumption is that all data studied in this paper satisfy this equation.

Before proceeding, it should be noted that if our boundary data corresponds to $G = 0$ then the only possible (nonzero) choice for ϕ is $\phi(z) = Cif(z)$, for some nonzero $C \in \mathbf{R}$. This implies that the null space corresponding to the infinite system in (3) is one dimensional and the eigenvector spanning this space is given by $a_k = c_k, k = 1, 2, 3, \cdots$ where $f(z) = \sum_{k=1}^{\infty} c_k z^k$.

3. Compact Operators. Taking real and imaginary parts of equation (3) gives us

$$\alpha_j + \sum_{k=1}^{\infty} k(\eta_{k+j-1}\alpha_k + \gamma_{k+j-1}\beta_k) = B_j, \quad j = 1, 2, 3, \ldots \tag{4}$$

$$\beta_j + \sum_{k=1}^{\infty} k(\gamma_{k+j-1}\alpha_k - \eta_{k+j-1}\beta_k) = C_j, \quad j = 1, 2, 3, \ldots \tag{5}$$

where we have used the notation $a_k = \alpha_k + i\beta_k$, $h_k = \eta_k + i\gamma_k$, and $A_k = B_k + iC_k$. For visualization purposes, we combine equations (4) and (5) into a doubly infinite matrix equation in which the two sums are combined into a block Hankel matrix composed with a diagonal matrix. In fact, (4) and (5) can be written as

$$(I_\infty + H_{r,\infty}D_\infty)\underline{\alpha} + H_{i,\infty}D_\infty\underline{\beta} = \underline{B} \tag{6}$$

$$(I_\infty - H_{r,\infty}D_\infty)\underline{\beta} + H_{i,\infty}D_\infty\underline{\alpha} = \underline{C} \tag{7}$$

so that

$$\left(\begin{pmatrix} I_\infty & 0 \\ 0 & I_\infty \end{pmatrix} + \begin{pmatrix} H_{r,\infty} & H_{i,\infty} \\ H_{i,\infty} & -H_{r,\infty} \end{pmatrix}\begin{pmatrix} D_\infty & 0 \\ 0 & D_\infty \end{pmatrix}\right)\begin{pmatrix} \underline{\alpha} \\ \underline{\beta} \end{pmatrix} = \begin{pmatrix} \underline{B} \\ \underline{C} \end{pmatrix} \tag{8}$$

where $\underline{\alpha} = (\alpha_1, \alpha_2, \ldots)^T$, $\underline{\beta} = (\beta_1, \beta_2, \ldots)^T$, $\underline{B} = (B_1, B_2, \ldots)^T$, $\underline{C} = (C_1, C_2, \ldots)^T$, I_∞ is the infinite identity matrix, $D_\infty = diag(1, 2, \ldots)$, $H_{r,\infty}$ is an infinite Hankel matrix generated by the η_k, and $H_{i,\infty}$ is an infinite Hankel matrix generated by the γ_k.

Now suppose $(\underline{\alpha}, \underline{\beta})$ represents a solution to (4),(5). Define

$$\underline{x} = \begin{pmatrix} D_\infty^{1/2}\underline{\alpha} \\ D_\infty^{1/2}\underline{\beta} \end{pmatrix}, \quad \underline{r} = \begin{pmatrix} D_\infty^{1/2}\underline{B} \\ D_\infty^{1/2}\underline{C} \end{pmatrix}.$$

Then (8) can be written as

$$(I_\infty + M_\infty)\,\underline{x} = \underline{r} \tag{9}$$

where M_∞ is given by

$$M_\infty = \begin{pmatrix} M_{r,\infty} & M_{i,\infty} \\ M_{i,\infty} & -M_{r,\infty} \end{pmatrix} = \begin{pmatrix} D_\infty^{1/2} H_{r,\infty} D_\infty^{1/2} & D_\infty^{1/2} H_{i,\infty} D_\infty^{1/2} \\ D_\infty^{1/2} H_{i,\infty} D_\infty^{1/2} & -D_\infty^{1/2} H_{i,\infty} D_\infty^{1/2} \end{pmatrix}.$$

Note that M_∞ is symmetric. We would now like to justify the formal manipulations above and show that M_∞ is a compact operator. This will require the following two preliminary lemmas.

Lemma 1. *Let f be a conformal map from the unit disk to the region Ω with boundary Γ. Let Γ be analytic and*

$$f(e^{i\theta})/\overline{f'(e^{i\theta})} = \sum_{k=-\infty}^{\infty} h_k e^{ik\theta}.$$

Then there exists a $C > 0$ and $R < 1$ such that

$$|h_k| \leq CR^{|k|}. \tag{10}$$

Proof: Since Γ is analytic, f extends as a bounded, analytic function with $f'(z) \neq 0$ for $|z| \leq 1/R$ for some $R < 1$. Let

$$f(z) = \sum_{k=1}^{\infty} c_k z^k \quad \text{and} \quad 1/f'(z) = \sum_{j=0}^{\infty} d_j z^k.$$

Then there is a c such that $|c_k|$, $|d_k| \leq cR^k$. Further, we have that

$$\begin{aligned} f(e^{i\theta})/\overline{f'(e^{i\theta})} &= \sum_{k=1}^{\infty}\sum_{j=0}^{\infty} c_k \overline{d}_j e^{i(k-j)\theta} \\ &= \sum_{l=1}^{\infty}\sum_{j=0}^{\infty} c_{l+j}\overline{d}_j e^{il\theta} + \sum_{l=0}^{\infty}\sum_{j=l+1}^{\infty} c_{j-l}\overline{d}_j e^{-il\theta} \\ &= \sum_{l=1}^{\infty}\sum_{j=0}^{\infty} c_{l+j}\overline{d}_j e^{il\theta} + \sum_{l=0}^{\infty}\sum_{j=1}^{\infty} c_j\overline{d}_{l+j} e^{-il\theta}. \end{aligned}$$

And so

$$|h_l| = |\sum_{j=0}^{\infty} c_{l+j}\overline{d}_j| \leq \sum_{j=0}^{\infty} |c_{l+j}||\overline{d}_j| \leq cR^l \sum_{j=0}^{\infty} R^{2j} = \frac{cR^l}{1-R^2} = CR^l, \quad l \geq 1.$$

Similarly

$$|h_{-l}| = |\sum_{j=1}^{\infty} c_j \overline{d}_{l+j}| \leq CR^l, \quad l \geq 0.$$

Next we show that the entries of $M_{r,\infty}$ and $M_{i,\infty}$ also decay exponentially fast.

Lemma 2. *Under the assumptions of Lemma 1, the (j,k)th entries of $M_{r,\infty}$ and $M_{i,\infty}$ decay like $cr^{|j+k|}$ for some $c > 0$ and $r < 1$.*

Proof: We will prove the case for $M_{r,\infty}$. The case for $M_{i,\infty}$ follows similarly. Let $m_{k,j}$ denote the (k,j)th entry of $M_{r,\infty}$. Then we must have $m_{k,j} = \sqrt{kj}\eta_{k+j-1}$. Therefore

$$|m_{k,j}| = \sqrt{kj}|h_{k+j-1}| \leq C\sqrt{kj}R^{|k+j|}. \tag{11}$$

Let $r = (1+R)/2 < 1$. Since

$$\lim_{x\to\infty} \frac{1}{\sqrt{x}}(\frac{r}{R})^x = \infty,$$

there exists an $l_0 \geq 0$ such that

$$\sqrt{l}R^l \leq r^l, \quad \forall l \geq l_0.$$

Let

$$c = \max_{0\leq l\leq l_0} \{\sqrt{l}(\frac{R}{r})^l\},$$

we then see that

$$\sqrt{l}R^l \leq cr^l, \quad \forall l \geq 0.$$

The lemma now follows directly from (11).

Lemma 2 gives us the following theorem and corollary.

Theorem 1. *$M_{r,\infty} : l^1 \to l^1$ and $M_{i,\infty} : l^1 \to l^1$ are compact operators where for $\underline{y} \in l^1$,*

$$M_{i,\infty}\underline{y} = \sum_{k=1}^{\infty} \sqrt{kj}\eta_{k+j-1}y_k, \quad j = 1,2,\ldots \tag{12}$$

$$M_{r,\infty}\underline{y} = \sum_{k=1}^{\infty} \sqrt{kj}\gamma_{k+j-1}y_k, \quad j = 1,2,\ldots \tag{13}$$

Proof: We will prove the theorem for $M_{r,\infty}$. As above, $M_{i,\infty}$ follows similarly. Define the finite rank operators $\{M_{r,n}\} = \{D_n^{1/2}H_nD_n^{1/2}\}$ by

$$M_{r,n}\underline{y} = \sum_{k=1}^{n} \sqrt{kj}\eta_{k+j-1}y_k, \quad j = 1,2,\ldots,n \tag{14}$$

for all $\underline{y} = (y_1, y_2, \ldots) \in l^1$. The goal is to show that $M_{r,\infty}$ can be approximated in the uniform norm by these finite rank operators.

If $A = (a_{kj})$ is an infinite matrix, then the induced l^1 operator norm is given by

$$||A|| = \sup_j \sum_{k=1}^{\infty} |a_{kj}|.$$

From the geometric decay of Lemma 2 we may write

$$\sum_{k=1}^{\infty} |m_{k,j}| \leq Cr^j \sum_{k=1}^{\infty} r^k \leq C_1 r^j, \quad j \geq 1.$$

Consequently,

$$\begin{aligned} ||M_{r,\infty} - M_{r,n}|| &= \sup \left\{ \sum_{k=1}^{\infty} |m_{k,n+1}|, \sum_{k=1}^{\infty} |m_{k,n+2}|, \dots \right\} \\ &\leq C_1 \sup\{r^{n+1}, r^{n+2}, \dots\} \\ &= C_1 r^{n+1} \to 0. \end{aligned}$$

Thus, $M_{r,\infty}$ is compact as desired.

Corollary 1. *M_∞ is compact on $l^1 \times l^1$ where for $\underline{x} = (\underline{x}^1, \underline{x}^2) \in l^1 \times l^1$,*

$$M_\infty \begin{pmatrix} \underline{x}^1 \\ \underline{x}^2 \end{pmatrix} = \begin{pmatrix} \sum_{k=1}^{\infty} \sqrt{kj}\eta_{k+j-1} x^1{}_k + \sum_{k=1}^{\infty} \sqrt{kj}\gamma_{k+j-1} x^2{}_k \\ \sum_{k=1}^{\infty} \sqrt{kj}\eta_{k+j-1} x^1{}_k - \sum_{k=1}^{\infty} \sqrt{kj}\gamma_{k+j-1} x^2{}_k \end{pmatrix}. \tag{15}$$

The norm on $l^1 \times l^1$ is given by

$$||\underline{x}||_{l^1 \times l^1} = ||\underline{x}^1||_{l^1} + ||\underline{x}^2||_{l^1}.$$

Proof: From the notation of the problem, it is easily verified that

$$||M_\infty - M_n||_{l^1 \times l^1} \leq 2(||M_{r,\infty} - M_{r,n}||_{l^1} + ||M_{i,\infty} - M_{i,n}||_{l^1})$$

The result follows from Theorem 1.

Next, we discuss the discretization of (9). Since M_∞ is compact and the matrix-vector multiplications can be performed rapidly, we will solve the discrete (normal) equations using the conjugate gradient method on the subspace orthogonal to the one dimensional null space.

4. Discretization. The natural choice for discretization is to truncate the sums given in (15) to n. This will lead to finite linear systems. However, in practice one

does not have the exact Fourier coefficients. If the conformal map f is known explicitly, we approximate the h_k's by evaluating $d(z) := f(z)/\overline{f'(z)}$ at the N Fourier points, $z = e^{ij\pi/N}, j = 0, 1, \cdots, N-1$, and taking the $N-$point FFT. In this case, the discrete $h_1, \cdots, h_n$, decay at a similar rate to the exact h_k (see [He, eq. 13.2-8, p. 20].) However, since the discrete Fourier coefficients are $N - periodic, h_k = h_{k-N}$, the remaining coefficients $h_{n+1} = h_{-n+1}, \cdots, h_{N-1} = h_{-1}$ do not decay geometrically. We just set $h_k = 0, k > n$ to insure geometric decay. When f is not known exactly, we use a numerical approximation at the N Fourier points given by Wegmann's method, as discussed in section 5, and again set $h_k = 0$ for $k = n+1, \cdots, N-1$. To avoid introducing more notation, we now let h_k, A_k, etc., denote the discrete Fourier coefficients.

The notation is similar to the infinite dimensional case:

$$D_n = diag(1, 2, \ldots, n),$$

$$\underline{\alpha} = (Re\ a_1, \ldots, Re\ a_n)^T, \quad \underline{\beta} = (Im\ a_1, \ldots, Im\ a_n)^T,$$

$$\underline{B} = (Re\ A_1, \ldots, Re\ A_n)^T, \quad \underline{C} = (Im\ A_1, \ldots, Im\ A_n)^T,$$

$$\underline{x} = \begin{pmatrix} D_n^{1/2}\underline{\alpha} \\ D_n^{1/2}\underline{\beta} \end{pmatrix}, \quad \underline{r} = \begin{pmatrix} D_n^{1/2}\underline{B} \\ D_n^{1/2}\underline{C} \end{pmatrix},$$

and

$$H_n = \begin{pmatrix} H_{r,n} & H_{i,n} \\ H_{i,n} & -H_{r,n} \end{pmatrix}.$$

Then analogously to the infinite system we have

$$M_n = \begin{pmatrix} M_{r,n} & M_{i,n} \\ M_{i,n} & -M_{r,n} \end{pmatrix} = \begin{pmatrix} D_n^{1/2}H_{r,n}D_n^{1/2} & D_n^{1/2}H_{i,n}D_n^{1/2} \\ D_n^{1/2}H_{i,n}D_n^{1/2} & -D_n^{1/2}H_{i,n}D_n^{1/2} \end{pmatrix},$$

so that our problem is to solve

$$(I_n + M_n)\underline{x} = \underline{r}. \tag{16}$$

Recall that $\underline{x}$ is subject to a uniqueness condition. Since $f'(0) > 0$, the condition $Im(a_1/f'(0)) = 0$ implies $x_{n+1} = 0$. Clearly, the (k,j)th entry of $M_{r,n}$ and $M_{i,n}$ are respectively $\sqrt{kj}Re(h_{k+j})$ and $\sqrt{kj}Im(h_{k+j})$.

We have computed the eigenvalues of M_n for the examples in section 5 using MATLAB. Note that if μ is an eigenvalue of M_n, then $-\mu$ is also an eigenvalue. We also find that -1 is an eigenvalue of M_n the rest of the eigenvalues decay rapidly to 0. The decay is due to the compactness of M_∞ shown in Corollary 1 of section 3. By [An], the spectrum of M_n is near to the spectrum of M_∞ for large n. We solve the normal equations, since $(I_n + M_n)^2$ is positive semidefinite.

Recall that our infinite system (9) has a one dimensional null space. The null space is generated by the null vector,

$$\underline{v} = (-Im\ c_1, -\sqrt{2}Im\ c_2, \ldots, -\sqrt{k}Im\ c_k, \ldots, Re\ c_1, \sqrt{2}Re\ c_2, \ldots, \sqrt{k}Re\ c_k, \ldots)^T.$$

In the discrete case, we find that for large n

$$\underline{v} = (-Im\ c_1, -\sqrt{2}Im\ c_2, \ldots, -\sqrt{n}Im\ c_n, Re\ c_1, \sqrt{2}Re\ c_2, \ldots, \sqrt{n}Re\ c_n)^T$$

satisfies $(I_n + M_n)\underline{v} = \underline{0}$ to within discretization error using our discrete approximations to the c_k's. It follows that our solution can be decomposed as

$$\underline{y} = \underline{x} + \delta\underline{v}. \tag{17}$$

It is clear from the conjugate gradient algorithm that if the initial guess $\underline{x}^{(0)}$ is in $\underline{v}^\perp$ then subsequent iterates $\underline{x}^{(q)}$ will be in $\underline{v}^\perp$. We take $\underline{x}^{(0)} = \underline{0}$. Conjugate gradient will then find $\underline{x} \in \underline{v}^\perp$ and imposing the uniqueness condition $y_{n+1} = 0$ will give us δ. By the results above, $(I_n + M_n)^2$ restricted to $\underline{v}^\perp$ is positive definite for sufficiently large n, since the second smallest eigenvalue of $I_\infty + M_\infty$ is bounded away from 0. Therefore conjugate gradient can be applied to the normal equations and the method will converge superlinearly.

In addition, we note that the matrix-vector multiplication involving the matrix M_n can be done efficiently using FFTs. In fact, for any n—vector $\underline{y}$, since D_n is diagonal, $D_n^{1/2}\underline{y}$ can be computed in n operations. Moreover, the matrix-vector multiplication $H\underline{y}$, where H is the Hankel matrix $H_{n,r}$ or $H_{n,i}$, can be computed in $O(N \log N)$ by using FFTs. The idea is to compute $T\underline{s} = (HJ)(J\underline{y})$ where J is the reversion matrix with ones on the anti-diagonal and T is a Toeplitz matrix (constant along diagonals). Next we imbed T into a matrix C as follows

$$C = \begin{pmatrix} T & X \\ X & T \end{pmatrix},$$

where X is chosen to make C circulant. Now C can be decomposed as $C = F^*\Lambda F$ where F is the N—point Fourier matrix and Λ is a diagonal matrix containing the eigenvalues of C. For more details on fast methods for Hankel and Toeplitz matrices see, e.g., [CN].

5. Numerical examples. In examples (i), (ii), and (iii) below, we choose $\phi(\zeta) = \zeta^3$, and $\chi(\zeta) = 0$. Then $u(\eta, \mu) = \eta^4 - \mu^4$. Note that, for the conformal map $f(z)$ from the disk, $\phi(z) = (f(z))^3$ and the boundary values at the mesh points are given by $G(z) = 4(Ref(z))^3 - i4(Imf(z))^3$. The discretization error in the Tables is given by the sup norm

$$\max_{0 \le j \le N-1} |\phi(e^{i2\pi j/N}) - \phi_n(e^{i2\pi j/N})|,$$

where ϕ_n is our nth degree approximation to ϕ. For analytic curves, this error behaves similarly to the discretization error for the conformal map which is $O(R^N)$ with R as given in Lemma 1; see [De] for a discussion of the accuracy of the conformal mapping methods.

We use the FFT method in [Weg] to find the approximate conformal map f. Wegmann approximates f by solving a discrete interpolation problem on the unit disk: Find $P_{n+1}(z)$, a polynomial of degree $n+1$, such that $P_{n+1}(e^{i2\pi j/N}) \in \Gamma, j = 0, \ldots, N-1$ with the normalization that the $P_{n+1}(0)$ is fixed and the coefficients of z and z^{n+1} are real. He computes this polynomial by applying a Newton method to find a discrete approximation

to the boundary correspondence. The linear systems may be solved by the conjugate gradient method in $O(N \log N)$ per step. Quadratic convergence of the Newton iterations and convergence of the polynomial to the conformal map as N increases for sufficiently smooth Γ is proven. Numerical experiments indicate that this method is among the most robust and reliable of the Fourier series methods on the disk [De].

For examples where the exact f is known, $d = f/\overline{f'}$ may be computed with either the exact or the approximate f. This seems to make little difference in the calculations if the approximate f is sufficiently accurate. The timings for finding the approximate f using [Weg] are usually only slightly greater than the timings given in the Tables for solving the boundary value problem for a given N.

In the Tables below, *iter* is the number of iterations required by conjugate gradient for the residuals to be $\leq 10^{-14}$. The computations were done in double precision on the WSU IBM ES9121 Model 440 mainframe computer and some rough timings are given. (Figures 1 and 2 and some of our examples were also done in MATLAB with similar results.) Stopping the iterations after the level of discretization error has been achieved could further reduce the timings, though not dramatically for these examples of very fast superlinear convergence. Note that as the minor-to-major axis ratio α of a region decreases toward 0 (that is, as R in Lemma 1 increases to 1), the convergence rate of the conjugate gradient method decreases. In our examples below, R may be taken as the distance from the origin to the nearest singularity of f and the connection with the minor-to-major aspect ratio is known [De]. In a future paper we will show how the convergence rate of the conjugate gradient method depends on the smoothness of the boundary Γ.

Other cases were also tried successfully, such as the simple examples in [KK]. If the biharmonic function has too simple a Goursat representation, the iterations may converge artificially fast. For instance, if $u(\eta, \mu) = \eta^2 + \eta\mu + \mu^2$, then $\phi(z) = f(z)$ and convergence is achieved in one iteration if N is large enough. On the other hand, note that the 5-to-1 ellipse in [GGMa, Table 3] is a difficult region for the conformal map from the disk and would require large N.

Example (i), inverted ellipse. Here $\Gamma : \gamma(\sigma) = \rho(\sigma)e^{i\sigma}$ where $\rho(\sigma) = \sqrt{1 - (1-\alpha^2)\sin^2\sigma}$ for $0 \leq \sigma \leq 2\pi$ and $0 < \alpha \leq 1$. This map is derived by inverting the familiar Joukowski map to the exterior of an ellipse. We have

$$f(z) = \frac{2\alpha z}{1 + \alpha - (1-\alpha)z^2}.$$

See Table 1 for results. Notice how *iter* is roughly independent of N but increases with α in our examples.

Table 1. Inverted ellipse with exact map and conjugate gradient

α	N	discr. error	iter	CPU sec
.8	32	$.5 \cdot 10^{-5}$	4	.2
.8	64	$.5 \cdot 10^{-12}$	3	.2
.8	128	$.5 \cdot 10^{-14}$	3	.2
.4	64	$.1 \cdot 10^{-3}$	6	.2
.4	128	$.6 \cdot 10^{-9}$	4	.2
.4	256	$.1 \cdot 10^{-13}$	4	.3
.2	128	$.2 \cdot 10^{-3}$	6	.3
.2	256	$.2 \cdot 10^{-8}$	4	.3
.2	512	$.3 \cdot 10^{-13}$	4	.4

Example (ii), arctanh. Here the conformal map is given by $f(z) = \log((1+rz)/(1-rz)), 0 < r < 1$, which maps the disk to increasingly elongated, cigar-shaped regions as $r \uparrow 1$. This map is perhaps the simplest example of a conformal map exhibiting the exponential crowding [De]. Figure 1 shows roughly 7 outlying eigenvalues for $\alpha = .49$ so that one would expect conjugate gradient to take about 7 iterations to converge as shown in Table 2. Also note the semilog plot in Figure 2 that shows the superlinear convergence behavior of the residuals.

Table 2. Arctanh regions with exact map and conjugate gradient

$\alpha(r)$	N	discr. error	iter	CPU sec
.84 (.5)	32	$.4 \cdot 10^{-4}$	6	.2
.84 (.5)	64	$.4 \cdot 10^{-9}$	4	.2
.84 (.5)	128	$.1 \cdot 10^{-13}$	4	.2
.49 (.9)	128	$.6 \cdot 10^{-3}$	8	.4
.49 (.9)	256	$.4 \cdot 10^{-6}$	6	.3
.49 (.9)	512	$.4 \cdot 10^{-12}$	6	.5
.29 (.99)	512	$.4 \cdot 10^{-1}$	14	.9
.29 (.99)	1024	$.2 \cdot 10^{-2}$	13	1.5
.29 (.99)	2048	$.6 \cdot 10^{-5}$	12	2.8
.29 (.99)	4096	$.1 \cdot 10^{-9}$	12	6.0

Example (iii), ellipse. Here $\Gamma : \gamma(\sigma) = \rho(\sigma)e^{i\sigma}$ where $\rho(\sigma) = \alpha/\sqrt{1-(1-\alpha^2)\cos^2\sigma}$ for $0 \leq \sigma \leq 2\pi$ and $0 < \alpha \leq 1$. The exact map can be given in terms of an elliptic integral.

This case also exhibits exponential crowding [De]. We approximate the f with [Weg].

Table 3. Ellipses with approximate map and conjugate gradient

α	N	discr. error	iter	CPU sec
.8	32	$.7 \cdot 10^{-3}$	6	.2
.8	64	$.5 \cdot 10^{-6}$	4	.2
.8	128	$.4 \cdot 10^{-12}$	3	.2
.8	256	$.2 \cdot 10^{-13}$	3	.3
.6	128	$.6 \cdot 10^{-3}$	8	.3
.6	256	$.3 \cdot 10^{-6}$	6	.4
.6	512	$.2 \cdot 10^{-12}$	3	.4
.4	2048	$.3 \cdot 10^{-4}$	10	2.6
.4	4096	$.7 \cdot 10^{-10}$	8	4.6

Acknowledgements. The authors thank Rudolf Wegmann for providing a copy of his Fortran code based on [Weg].

References

[An] P. M. Anselone, *Collectively Compact Operator Approximation Theory,* Prentice-Hall, Inc., 1971.

[CN] R. H. Chan and M. K. Ng, *Conjugate gradient methods for Toeplitz systems,* to appear in SIAM Review.

[Con] J. B. Conway, *A Course in Functional Analysis, 2nd ed.,* Springer-Verlag, 1990.

[De] T. K. DeLillo, *The accuracy of numerical conformal mapping methods: a survey of examples and results,* SIAM J. Numer. Anal., 31 (1994) 788–812.

[DE] T. K. DeLillo and A. R. Elcrat, *A Fornberg-like conformal mapping method for slender regions,* J. Comput. Appl. Math., 46 (1993) 49–64.

[DEP] T. K. DeLillo, A. R. Elcrat, and J. A. Pfaltzgraff, *Numerical conformal mapping methods based on Faber series,* submitted for publication.

[Ga] D. Gaier, *Konstruktive Methoden der konformen Abbildung,* Springer-Verlag, Berlin, Gottingen, Heidelberg, 1964.

[GVL] G. Golub, C. Van Loan, *Matrix Computations, 2nd ed.,* John Hopkins U. Press, 1989.

[GGMa] A. Greenbaum, L. Greengard, and A. Mayo, *On the numerical solution of the biharmonic equation in the plane,* Physica D, 60 (1992) 216–225.

[He] P. Henrici, *Applied and Computational Complex Analysis, Vol. III,* John Wiley, New York, 1986.

[KK] L. V. Kantorovich and V. I. Krylov, *Approximate Methods of Higher Analysis,* P. Noordhoff Ltd, Groningen, The Netherlands, 1958.

[K] A. Karageorghis, *The method of fundamental solutions for the solution of steady-state free boundary problems,* J. Comput. Phys., 98 (1992) 119–128.

[MG] A. Mayo and A. Greenbaum, *Fast parallel iterative solution of Poisson's and the biharmonic equation on irregular regions,* SIAM J. Sci. Stat. Comput., 13 (1992) 101–118.

[Mik] S. G. Miklin, *Integral Equations,* MacMillan Co., New York, 1964.

[MT] L. M. Milne–Thomson, *Theoretical Hydrodynamics, 5th edition,* MacMillan Press, London, 1968.

[Musk] N. I. Muskhelishvili, *Some Basic Problems of the Mathematical Theory of Elasticity,* P. Noordhoff Ltd, Groningen, Holland, 1953.

[Poz] C. Pozrikidis, *Boundary Integral and Singularity Methods for Linearized Viscous Flow,* Cambridge U. Press, 1992.

[Weg] R. Wegmann, *Discrete Riemann-Hilbert problems, interpolation of simply closed curves, and numerical conformal mapping,* J. Comput. Appl. Math., 23 (1988) 323–352.

Figure captions

Figure 1. Eigenvalue distribution for example ii).

Figure 2. Convergence of residuals for 10 iterations of the conjugate gradient method for example ii).

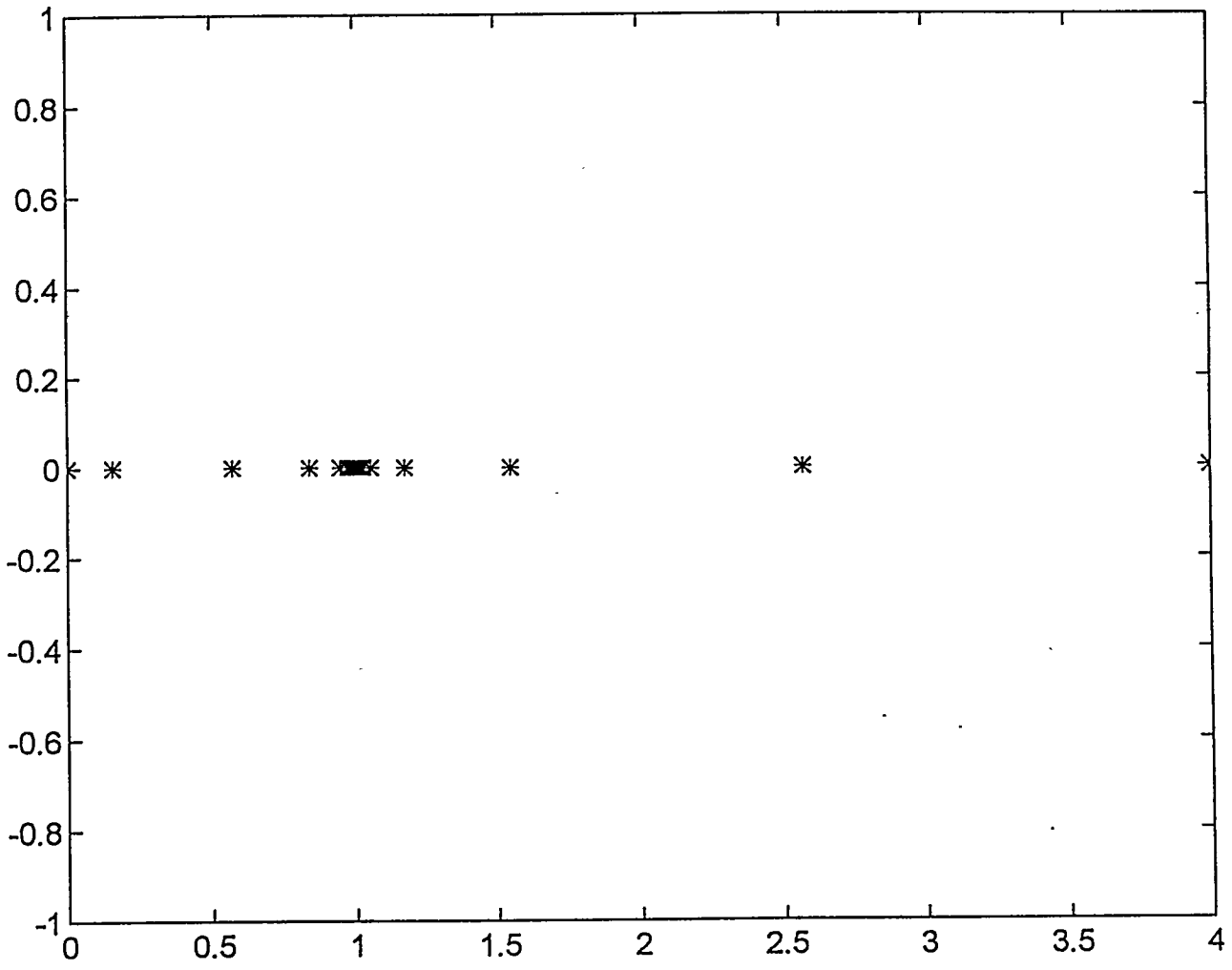

Fig. 1.

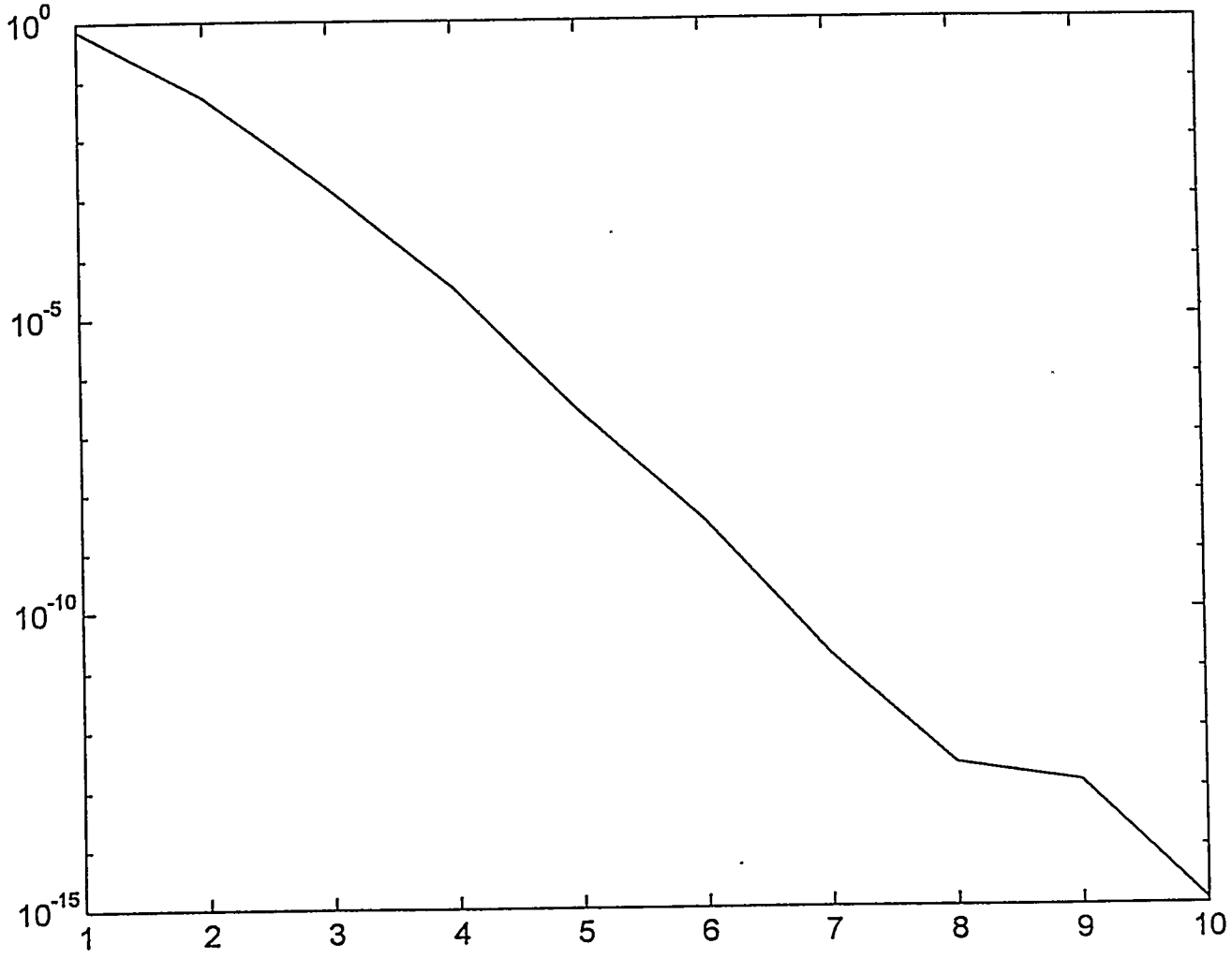

Fig. 2.